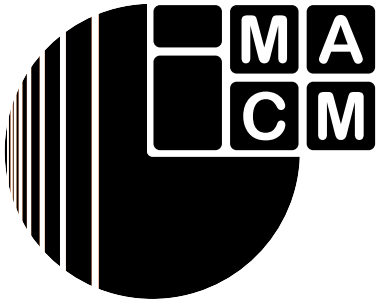

Bergische Universität Wuppertal

Fachbereich Mathematik und Naturwissenschaften

Institute of Mathematical Modelling, Analysis and Computational Mathematics (IMACM)

Preprint BUW-IMACM 16/16

Christian Hendricks, Matthias Ehrhardt and Michael Günther

Hybrid finite difference / pseudospectral methods for the Heston and Heston-Hull-White PDE

August 15, 2016

http://www.math.uni-wuppertal.de

Hybrid finite difference / pseudospectral methods for the Heston and Heston-Hull-White PDE

Christian Hendricks, Matthias Ehrhardt and Michael Günther

Bergische Universität Wuppertal, Chair of Applied Mathematics and Numerical Analysis (AMNA), Gaußstraße 20, 42119 Wuppertal, Germany. Email: {hendricks,ehrhardt,guenther}@math.uni-wuppertal.de

August 6, 2016

In this article we propose a hybrid spatial finite difference / pseudospectral discretization for European option pricing problems under the Heston and Heston-Hull-White model. In direction of the underlying asset, where the payoff profile is non-smooth, we use a standard central second-order finite difference scheme, whereas we use a Chebyshev collocation method in the other spatial dimensions. In the time domain we employ alternating direction implicit schemes to efficiently decompose the system matrix into simpler one dimensional problems. This approach allows to compute numerical solutions, which are second-order accurate in time and exhibit spectral accuracy in the spatial domains except for the asset direction. The numerical experiments reveal that the proposed scheme outperforms the standard second-order finite difference scheme in terms of accuracy versus run-time and shows an unconditionally stable behavior.

Keywords— stochastic volatility models, Heston, Heston-Hull-White, spectral method, finite differences, alternating direction implicit

1 Introduction

The pricing of derivatives in financial engineering is in general based on modeling a stochastic differential equation (SDE) system, which describes the main factors driving equity markets. In the seminal paper by Black and Scholes (1973) the asset price is given by a stochastic diffusion process. More advanced models also incorporate additional risk factors, such as the asset's volatility and the risk-free interest rate. These models are able to capture the behavior, which we observe in financial markets, in a much more realistic way, e.g., they can reflect volatility smiles or model the impact of fluctuating interest rates. In this article we consider the Heston model (Heston (1993)) as a testbed for two factor models and the three dimensional Heston-Hull-White (HHW) model as a testbed for three factor models.

The Heston partial differential equation (PDE) is given by

$$\frac{\partial u}{\partial t} = \frac{1}{2}s^2 v\frac{\partial^2 u}{\partial s^2} + \rho_{12}\sigma_1 sv\frac{\partial^2 u}{\partial s\partial v} + \frac{1}{2}\sigma_1^2 v\frac{\partial^2 u}{\partial v^2} + rs\frac{\partial u}{\partial s} + \kappa(\eta - v)\frac{\partial u}{\partial v} - ru, \tag{1}$$

for inverse time $t \in [0,T]$, asset $s \in [0,\infty)$ and volatility $v \in [0,\infty)$. The risk-less interest rate is denoted by r and the volatility of the volatility by σ_1. The long-term mean of v is given by η, while κ denotes the mean reversion rate of v. The correlation between the asset and the volatility is given by ρ_{12}. At the maturity $t = 0$ the option holder obtains the following payoff for an European put option

$$u(s,v,0) = \max\{K - s, 0\},$$

where K is the strike price. In some simple cases the Heston model can be solved via closed-form analytical formulas, for example in the constant coefficient case for European options. However, for more complicated settings numerical techniques have to be applied. The Heston-Hull-White model is an extension of the Heston model, where the interest rate is assumed to follow a mean-reverting process. The option value is assumed to satisfy the PDE

$$\begin{aligned}\frac{\partial u}{\partial t} =& \frac{1}{2}s^2 v\frac{\partial^2 u}{\partial s^2} + \frac{1}{2}\sigma_1^2 v\frac{\partial^2 u}{\partial v^2} + \frac{1}{2}\sigma_2^2\frac{\partial^2 u}{\partial r^2} \\ &+ \rho_{12}\sigma_1 s v\frac{\partial^2 u}{\partial s\partial v} + \rho_{13}\sigma_2 s\sqrt{v}\frac{\partial^2 u}{\partial s\partial r} + \rho_{23}\sigma_1\sigma_2\sqrt{v}\frac{\partial^2 u}{\partial v\partial r} \\ &+ rs\frac{\partial u}{\partial s} + \kappa(\eta - v)\frac{\partial u}{\partial v} + a_r(b_r - r)\frac{\partial u}{\partial r} - ru, \end{aligned} \tag{2}$$

for inverse time $t \in [0,T]$, asset $s \in [0,\infty)$, volatility $v \in [0,\infty)$ and risk-free interest rate $r \in (-\infty,\infty)$. Compared to the Heston model, the HHW model has the following additional parameters: the volatility of the interest rate is σ_2; the long-term mean of r is given by b_r and its mean reversion rate by a_r; the correlation between s and r is denoted by ρ_{13} and between v and r by ρ_{23}. Similar to the payoff given above, the solution at expiry is

$$u(s,v,r,0) = \max\{K - s, 0\}.$$

In the literature several methods have been discussed to solve problems (1) and (2) for vanilla option pricing problems. They range from semi-closed approximations (Heston (1993); in't Hout et al. (2007)), Fourier-cosine (Fang and Oosterlee (2008); Grzelak and Oosterlee (2011)) and tree approaches (Florescu and Frederi (2005a,b); Briani et al. (2015, 2016)) to finite difference methods (Kluge (2002), in't Hout and Foulon (2010) and Haentjens and in't Hout (2012)). While semi-closed approximations and Fourier-cosine methods allow to compute option prices very fast, they rely on the availability of a closed formula of the characteristic function or an approximation to it, which can be computed with low computational effort. In case of the HHW model a semi-closed formula is available if ρ_{13} and ρ_{23} are equal to zero. If $\rho_{23} = 0$ only an approximation of the characteristic function is available. In contrast PDE techniques, such as finite difference schemes, are in general more expensive, but are advantageous in terms of general applicability. Finite difference methods have been proposed by various researchers. Kluge (2002) has solved the Heston PDE via second-order finite differences. In Kluge (2002), in't Hout and Foulon (2010) and Haentjens and in't Hout (2012) Alternating Direction Implicit (ADI) time stepping has been used to efficiently deal with the mixed derivative term. High-order compact finite differences were proposed by Düring and Fournie (2012), Düring et al. (2014). These schemes exploit the structure of the governing PDE to derive a fourth order approximation on the compact stencil. Also methods with a higher spatial accuracy were discussed by various researchers: Linde et al. (2005) employed broad stencils to approximate the PDE for option pricing with one and two underlying assets with sixth order accuracy and spectral methods were used by Pindza et al. (2013). The main drawback of high order methods is that the theoretical rate of accuracy is rarely seen in practice due to the non-smooth nature of the

solution or initial payoff profile, respectively. In Pooley et al. (2003) numerical techniques are discussed to recover a high rate of convergence, e.g., smoothing of the initial condition, concentrating grid points in the region of interest, etc. However, the discontinuity of the payoff profile for option pricing problems in general occurs in the direction of the underlying asset, while in direction of the other risk factors the solution is smooth. In this article we want to exploit this structure and propose a hybrid scheme, which uses a second-order central finite difference approximation in direction where the discontinuity occurs. In the other spatial dimensions we employ a high order Chebyshev spectral approximation.

The article is organized as follows: In section 2 we present the spatial discretization and give a brief introduction to Chebyshev collocation methods. In section 3 we discuss ADI time discretization and its stability properties for spectral spatial discretizations. Section 4 is devoted to the derivation of the hybrid scheme for the Heston and HHW model. In the last section we numerically test the proposed method in the time domain as well as in the spatial directions. Here, we are especially interested in its performance compared to a standard second-order finite difference approximation and we therefore perform a thorough run-time analysis.

2 Spatial discretization

In this section we derive the spatial approximation in terms of a method of lines approach. Hence, we rewrite the PDEs (1) and (2) into a semi-discrete system

$$U'(t) = FU(t), \quad t \geq 0, \tag{3}$$

with initial value $U(0) = U_0 \in \mathbb{R}^N$, where F is the real valued discretization matrix of the spatial derivatives of size $N \times N$. The resulting system of ordinary differential equations (ODEs) can then be solved by any suitable time discretization method.

2.1 Finite differences

The approximation of derivatives via finite differences is based on Taylor expansions under the assumption that the solution is sufficiently smooth. We consider a general smooth one dimensional function g on a uniform grid with spacing h. A symmetric approximation to the first and second derivative with an order of accuracy of two at the k-th grid node is given by

$$\begin{aligned} \tfrac{1}{2h}\left(g_{k+1} - g_{k-1}\right) &= \frac{\partial g}{\partial x}(x_k) + \mathcal{O}(h^2), \\ \tfrac{1}{h^2}\left(g_{k+1} - 2g_k + g_{k-1}\right) &= \frac{\partial^2 g}{\partial x^2}(x_k) + \mathcal{O}(h^2). \end{aligned}$$

These standard approximations of the first and second derivative can be written in matrix notation $G' \approx D_{FD}G$, $G'' \approx D_{FD}^2 G$, where $G = (g_1, g_2, ..., g_N)^\top$. Hereby D_{FD}, D_{FD}^2 are tridiagonal matrices.

2.2 Chebyshev interpolation and differentiation

In the smooth direction we propose a Chebyshev pseudospectral (CPS) collocation method to achieve highly accurate approximation with a low number of grid nodes. Similar to the finite difference case we illustrate the method by considering a smooth one dimensional

function g. Let the function values of g in the interval $[-1,1]$ be given at Chebyshev-Gauss-Lobatto points $x_j = \cos\frac{\pi j}{N}$, $j = 0,1,...,N$. In order to approximate the derivative firstly a Chebyshev interpolant interolation g_j at the grid nodes x_j is computed. In a second step the interpolant is differentiated to obtain an estimate of the derivative of the data. Let the interpolant be given in Lagrange form

$$p_N(x) = \sum_{j=0}^{N} g_j l_j(x),$$

with

$$l_j(x) = \prod_{\substack{i=0 \\ i\neq j}}^{N} \frac{x-x_i}{x_j-x_i}.$$

Then one can easily approximate the derivative at the grid nodes via

$$p'_N(x_i) = \sum_{j=0}^{N} g_j l'_j(x_i) = \sum_{j=0}^{N} d_{ij} g_j \qquad \text{for } i = 0,1,...,N.$$

This can be written in a more compact way in matrix notation $G' \approx D_{SP}G$, where $D_{SP} = (d_{ij})_{i,j=0,...,N}$ is the Chebyshev differentiation matrix with $d_{ij} = l'_j(x_i)$ for $i,j = 0,1,...,N$ and $G = (g_0, g_1, ..., g_N)^\top$. The second derivative can be derived in an analogue way by differentiating twice to obtain $D^2_{SP} = (\tilde{d}_{ij})_{i,j=0,...,N}$, with entries $\tilde{d}_{ij} = l''_j(x_i)$ for $i,j = 0,1,...,N$. Explicit formulas for the entries of the matrices for Chebyshev-Gauss-Lobatto points can be found in Gottlieb et al. (1984), Canuto et al. (2006).

This global interpolation approach has the advantage, that it is highly accurate if u fulfills certain smoothness conditions. This allows to use significant less grid nodes compared to low order methods. In the following we cite two theorems regarding the accuracy of Chebyshev interpolation given by Gil et al. (2007):

Theorem 3.12 in Gil et al. (2007) *When a function u has $m+1$ continuous derivatives on $[-1,1]$, where m is a finite number, then $|u(x) - p_N(x)| = \mathcal{O}(N^{-m})$ as $N \to \infty$ for all $x \in [-1,1]$.*

Theorem 3.13 in Gil et al. (2007) *When a function u on $x \in [-1,1]$ can be extended to a function that is analytic inside an ellipse E_r defined by*

$$E_r = \{z : |z + \sqrt{z^2-1}| = r\}, \quad r > 1,$$

then $|u(x) - p_N(x)| = \mathcal{O}(r^{-N})$ as $N \to \infty$ for all $x \in [-1,1]$.

Let us note that similar estimates also hold for the derivatives. Thus, we can expect a geometric error decay if u is sufficiently smooth, analytic, respectively. But the spectral accuracy does not come for free: the differentiation matrices are densely filled, which makes it very costly to solve the systems arising while using implicit time stepping. If explicit schemes are employed, step size restrictions of $\Delta_t = \mathcal{O}(N^{-2})$ for hyperbolic and $\Delta_t = \mathcal{O}(N^{-4})$ for diffusion problems lead to a large computational effort compared to second-order central finite differences, which only have restrictions of the form $\Delta_t = \mathcal{O}(N^{-1})$, $\Delta_t = \mathcal{O}(N^{-2})$.

3 Alternating Direction Implicit schemes

We consider the semi-discrete formulation (3)

$$U'(t) = FU(t), \quad t > 0,$$

supplied with suitable initial and boundary data and U depending only on the time t. The d dimensional spatial discretization F can be decomposed into

$$F = F_0 + F_1 + ... + F_d,$$

where F_0 stems from all mixed derivatives and F_i from each unidirectional contribution of coordinate direction $i = 1, ..., d$. With the help of ADI time stepping the equation system can be solved as a sequence of one dimensional problems, which significantly reduces the run-time compared to implicit Euler or Crank-Nicolson time marching. In the following we consider four well known ADI schemes.

Douglas scheme (DO):

$$\begin{cases} Y_0 & = U_n + \Delta_t F U_n, \\ Y_i & = Y_{i-1} + \theta \Delta_t \left(F_i Y_i - F_i U_n \right) \text{ for } i = 1, ..., d \\ U_{n+1} & = Y_d. \end{cases} \tag{4}$$

Craig-Sneyd scheme (CS):

$$\begin{cases} Y_0 & = U_n + \Delta_t F U_n, \\ Y_i & = Y_{i-1} + \theta \Delta_t \left(F_i Y_i - F_i U_n \right) \text{ for } i = 1, ..., d \\ \tilde{Y}_0 & = Y_0 + \frac{1}{2} \Delta_t \left(F_0 Y_d - F_0 U_n \right) \\ \tilde{Y}_i & = \tilde{Y}_{i-1} + \theta \Delta_t \left(F_i \tilde{Y}_i - F_i U_n \right) \text{ for } i = 1, ..., d \\ U_{n+1} & = \tilde{Y}_d. \end{cases} \tag{5}$$

Modified Craig-Sneyd scheme (MCS):

$$\begin{cases} Y_0 & = U_n + \Delta_t F U_n, \\ Y_i & = Y_{i-1} + \theta \Delta_t \left(F_i Y_i - F_i U_n \right) \text{ for } i = 1, ..., d \\ \hat{Y}_0 & = Y_0 + \theta \Delta_t \left(F_0 Y_d - F_0 U_n \right) \\ \tilde{Y}_0 & = \hat{Y}_0 + (\frac{1}{2} - \theta) \Delta_t \left(F Y_d - F U_n \right) \\ \tilde{Y}_i & = \tilde{Y}_{i-1} + \theta \Delta_t \left(F_i \tilde{Y}_i - F_i U_n \right) \text{ for } i = 1, ..., d \\ U_{n+1} & = \tilde{Y}_d. \end{cases} \tag{6}$$

Hundsdorfer-Verwer scheme (HV):

$$\begin{cases} Y_0 & = U_n + \Delta_t F U_n, \\ Y_i & = Y_{i-1} + \theta \Delta_t \left(F_i Y_i - F_i U_n \right) \text{ for } i = 1, ..., d \\ \tilde{Y}_0 & = Y_0 + \frac{1}{2} \Delta_t \left(F Y_d - F U_n \right) \\ \tilde{Y}_i & = \tilde{Y}_{i-1} + \theta \Delta_t \left(F_i \tilde{Y}_i - F_i Y_d \right) \text{ for } i = 1, ..., d \\ U_{n+1} & = \tilde{Y}_d, \end{cases} \tag{7}$$

where Δ_t is the step size in time, $U_n \sim U(n\Delta_t)$ and $\theta > 0$ is a real parameter. The Douglas method consists of one explicit Euler step and d one dimensional correction steps. The

scheme exhibits order two in time if $F_0 = 0$, $\theta = \frac{1}{2}$ and order one otherwise. The (modified) Craig-Sneyd and the Hundsdorfer-Verwer scheme are extensions of the DO scheme, where a second explicit step and an additional sweep of correction steps are performed. The Craig-Sneyd scheme exhibits order two in time if $\theta = \frac{1}{2}$ independent of F_0, while the latter two schemes have order two for arbitrary choices of θ. In general lower values for θ lead to more accurate solutions, but might cause instabilities if chosen too small. Hence, the value has to be chosen very carefully. Hundsdorfer (1999), Lanser et al. (2001), in't Hout and Welfert (2007), in't Hout and Welfert (2009), in't Hout and Mishra (2011), in't Hout and Mishra (2013) spent much effort on the stability analysis in the von Neumann framework. They consider a general convection diffusion equation with frozen coefficients

$$\frac{\partial u}{\partial t} = \operatorname{div}(A\nabla u) + c \cdot \nabla u,$$

with symmetric positive semi definite matrix $A = (a_{ij})$ and vector $c = (c_1, c_2, ..., c_d)^\top$. Let $z_i = \Delta_t \lambda_i$, where λ_i denotes the eigenvalue of the discretization operator F_i for $i = 0, 1, ..., d$. In the following we consider $d = 2$ and assume the condition

$$Re(z_1) \leq 0, \quad Re(z_2) \leq 0 \quad \text{and} \quad |z_0| \leq 2\gamma\sqrt{Re(z_1)Re(z_2)},$$

to hold for $z_0, z_1, z_2 \in \mathbb{C}$, where $\gamma \in [0, 1]$ describes the relative size of the mixed derivative coefficient

$$|a_{ij}| \leq \gamma\sqrt{a_{ii}a_{jj}} \quad \text{for all } i \neq j.$$

Then, according to in't Hout and Welfert (2007) the DO and CS scheme are stable for $\theta \geq \frac{1}{2}$. in't Hout and Mishra (2011) derive the necessary condition $\theta \geq \frac{2}{5}$, if $z_0 \in \mathbb{R}$, $z_1, z_2 \in \mathbb{C}$ and $\theta \geq \frac{5}{12}$, if $z_0, z_1, z_2 \in \mathbb{C}$ for the MCS scheme with $\gamma = 1$. In practice the scheme has been successfully applied to two dimensional problems by in't Hout and Foulon (2010) with the parameter choice $\theta = \frac{1}{3}$ under the condition that $\gamma \leq 0.96$. The HV scheme is unconditionally stable for $\theta \geq \frac{1}{2} + \frac{1}{6}\sqrt{3}$ if $z_1, z_2 \in \mathbb{C}$ and no mixed derivatives are present, see Lanser et al. (2001). In numerical experiments by in't Hout and Foulon (2010) this parameter choice for θ also led to a monotone error decay in the case of convection diffusion equations with mixed derivative terms. In the three dimensional case theoretical stability results are lacking in the literature. However, ADI schemes have been successfully applied to three dimensional problems by Haentjens and in't Hout (2012) using the θ values derived for pure diffusion equations in in't Hout and Welfert (2009): DO $\theta \geq \frac{2}{3}$, CS $\theta \geq \frac{1}{2}$, MCS $\theta \geq \max\{\frac{1}{3}, \frac{2}{13}(2\gamma + 1)\}$. For the HV scheme the bound derived for two dimensional convection-diffusion problems led to a stable behavior.

3.1 Stability considerations

In order to investigate the stability of the hybrid method we consider the general convection diffusion equation with fixed coefficients

$$\frac{\partial u}{\partial t} = \operatorname{div}(A\nabla u) + c \cdot \nabla u \text{ on } \Omega = [0, 1] \times [-1, 1], \ t > 0,$$

where $A = (a_{ij})$ is a symmetric positive semi definite matrix and $c = (c_1, c_2, ..., c_d)^\top$ the vector of convection coefficients. In the following we consider the two dimensional case $d = 2$. Let the mesh be given by a tensor based discretization of directions x, y via $x_i = i \cdot h$, $i = 1, 2, ..., N_x$ and $y_i = \cos(\frac{\pi \cdot i}{N_y})$ for $i = 0, 1, ..., N_y$. Using the notation of Kronecker products for matrices A of size $k_1 \times l_1$, B of size $k_2 \times l_2$

$$A \otimes B = \begin{pmatrix} a_{1\,1}B & \cdots & a_{1\,l_1}B \\ \cdots & & \\ a_{k_1\,1}B & \cdots & a_{k_1\,l_1}B \end{pmatrix},$$

the spatial discretization of the hybrid scheme can be written as

$$\begin{aligned} FU =& a_{11} D_{FD}^2 \otimes I_{N_y} U + (a_{12} + a_{21}) D_{FD} \otimes D_{SP} U + a_{22} I_{N_x} \otimes D_{SP}^2 U \\ &+ c_1 D_{FD} \otimes I_{N_y} U + c_2 I_{N_x} \otimes D_{SP} U, \end{aligned}$$

where I_{N_x}, I_{N_y} denote the identity matrix of size N_x, N_y+1, respectively. The vector $U \in \mathbb{R}^{N_x \cdot (N_y+1)}$ contains the function values at the grid nodes $U = (u_{0,1}, u_{0,2}, \ldots, u_{0,N_x}, u_{1,1}, \ldots, u_{N_y,N_x-1}, u_{N_y,N_x}) = (u(x_1, y_0), u(x_2, y_0), \ldots, u(x_{N_x}, y_0), u(x_1, y_1), \ldots, u(x_{N_x-1}, y_{N_y}), u(x_{N_x}, y_{N_y}))$. Then we decompose the system via

$$\begin{aligned} F_0 U &= (a_{12} + a_{21}) D_{FD} \otimes D_{SP} U, \\ F_1 U &= a_{11} D_{FD}^2 \otimes I_{N_y} U + c_1 D_{FD} \otimes I_{N_y} U, \\ F_2 U &= a_{22} I_{N_x} \otimes D_{SP}^2 U + c_2 I_{N_x} \otimes D_{SP} U. \end{aligned}$$

In a next step the ADI time discretization can be applied. For purposes of the stability investigations we rewrite methods (4) - (7) into the one step form

$$U_{n+1} = R U_n,$$

with iteration matrix R. The method is stable if $\|R\| \leq 1$ holds. In the literature in't Hout and Welfert (2007), in't Hout and Wyns (2016), Hendricks et al. (2016) it was shown that the iteration matrices are of the following form

$$R_{DO} = I + P^{-1} Z, \tag{8}$$

$$R_{CS} = I + P^{-1} Z + \tfrac{1}{2} P^{-1} Z_0 P^{-1} Z, \tag{9}$$

$$R_{MCS} = I + P^{-1} Z + P^{-1} (\theta Z + (\tfrac{1}{2} - \theta) Z) P^{-1} Z, \tag{10}$$

$$R_{HV} = (I + P^{-1} Z)^2 - P^{-1} (I + \tfrac{1}{2} Z) P^{-1} Z, \tag{11}$$

with $P = (I_{N_x} \otimes I_{N_y} - \theta \Delta_t F_1)(I_{N_x} \otimes I_{N_y} - \theta \Delta_t F_2)$, $Z_0 = \Delta_t F_0$, $Z = \Delta_t F_0 + \Delta_t F_1 + \Delta_t F_2$. One crucial property for stability of the ADI schemes is that the eigenvalues of the operators F_1 and F_2 have negative real parts. For central second-order finite differences this is clearly fulfilled, see in't Hout and Welfert (2007). In the case of Chebyshev spectral methods it was shown by Gottlieb and Lustman (1983) that the second derivative matrix has negative and distinct real valued eigenvalues, which are bounded by $\mathcal{O}(N_y^4)$. They prove this result for Dirichlet, Neumann and Robin boundary conditions (BCs). In Canuto et al. (2006) section 7.3.2 the eigenvalues of convection diffusion operators are analyzed for Dirichlet boundary conditions. Following their proof one directly observes that $Re(\lambda) \leq -a_{22} \frac{\pi^2}{4}$ and the spectral radius is bounded by $\mathcal{O}(N_y^4)$ due to the second derivative matrix. Numerical tests in Canuto et al. (2006) reveal that these bounds are sharp. In the case of convection diffusion problems with Neumann boundary conditions we numerically compute the eigenvalues of the generalized problem

$$QU = \lambda B U, \tag{12}$$

where Q is a $(N_y+1) \times (N_y+1)$ matrix, which consists of the matrix $D_{SP}^2 + D_{SP}$ at the inner nodes and the first and last row are identical to the first and last row of the differentiation matrix D_{SP} due to the homogeneous Neumann boundary conditions. The B matrix is identical to the identity matrix of size $(N_y+1) \times (N_y+1)$ except for the first and last entry, which is set to zero. Figure 1 shows the eigenvalues of problem (12), which has been solved using the QZ algorithm provided by the Matlab® routine $eig(.,.)$. One observes that the results for Dirichlet also hold for Neumann boundary conditions: except

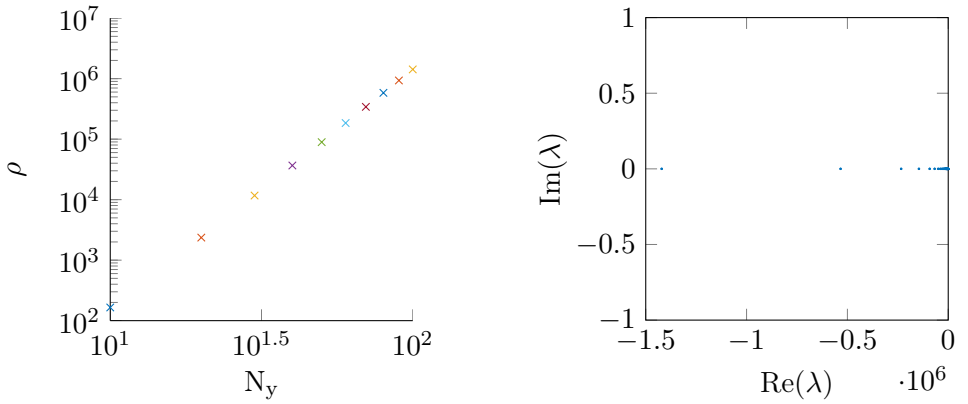

(a) Modulus of maximal eigenvalue of problem (12), slope 3.94.

(b) Eigenvalues of problem (12) with $N_y = 100$.

Figure 1: Neumann boundary conditions.

for one zero eigenvalue, all eigenvalues lie on the left-hand side of the complex plane and the spectral radius grows with $\mathcal{O}(N_y^4)$. The zero eigenvalue is associated with the eigenvector $u = c \cdot (1, ..., 1)^\top$ for an arbitrary constant c. These results ensure the stability if no mixed derivatives are present. Since in financial engineering mixed derivative terms arise due to the correlation structure between assets and/or risk factors it is important to include them in our stability considerations. Thus, we numerically compute the eigenvalues of the problem

$$RU = \lambda BU \tag{13}$$

with R given by (8) - (11). If Dirichlet boundary conditions are applied, then R is of size $N_x(N_y - 1) \times N_x(N_y - 1)$. In the second coordinate direction, where the Chebyshev collocation method is used the first and last row as well as the first and last column are removed due to the boundary condition. The matrix B is the identity matrix of appropriate size. If a homogeneous Neumann boundary condition is used in the second coordinate direction, we proceed according to the problem (12) to construct the differentiation matrices, which are employed to compute P. This matrix stems from all implicitly treated terms in the ADI method. For the explicit parts, namely Z_0 and Z, we proceed as follows: we compute the solution at the interior nodes and determine the boundary values in such a way that they satisfy the boundary condition by solving the system

$$d_{00}u_{k,0} + d_{0N_y}u_{k,N_y} = -\sum_{j=1}^{N_y-1} d_{0j}u_{k,j}$$

$$d_{N_y0}u_{k,0} + d_{N_yN_y}u_{k,N_y} = -\sum_{j=1}^{N_y-1} d_{N_yj}u_{k,j}$$

for $k = 1, ..., N_x$. Let $\tilde{D}$ denote the matrix which forces the boundary nodes in the y-direction to fulfill the boundary condition according to the system above, then we can compute the matrix stemming from the explicit time-stepping via $Z := \tilde{D}Z$ and $Z_0 := \tilde{D}Z_0$. Similar to problem (12) the matrix B is the identity matrix with zeros on the diagonal for each grid node lying on the boundary of y.

In the following we numerically investigate the stability of the ADI schemes. Therefore, we compute the spectrum of the iteration matrices R given by equations (8) - (11). If

$\rho(R) < 1$ is fulfilled the numerical scheme is stable. For our numerical experiment we consider the diffusion coefficient matrix and the convection vector

$$A = \begin{pmatrix} 1 & 1 \\ 1 & 1 \end{pmatrix}, \qquad c = \begin{pmatrix} 1 \\ 1 \end{pmatrix}.$$

The matrix A is symmetric positive semi-definite with the largest possible relative size of the mixed derivative coefficient ($\gamma = 1$). This choice can be seen as a worst case scenario in terms of the stability since the evolution of the solution in one variable is completely determined by the variable in the other coordinate direction. The ratio between convection and diffusion is equal to one for this parameter choice. In case of the MCS scheme we choose $\theta = 0.42$ since the eigenvalues of the approximation of the mixed derivative term are complex and since $\gamma = 1$. Further we let $\Delta_t = 0.1$ for our numerical evaluations. The θ value is chosen according to the values given in section 3 derived for finite difference schemes. Figures 2, 3 show the largest modulus of eigenvalue and the location of all eigenvalues in the complex plane of problem (13) with Dirichlet and Neumann boundary conditions. For an increasing number of grid nodes, the spectral radius for both problems approaches one from below. Thus, we expect a stable behavior of the hybrid scheme even for problems with large correlations. Please note, that one obtains similar results also for problems with strong convection dominance.

4 Heston and Heston-Hull-White model

This section is devoted to the derivation of the hybrid FD/CPS discretization for the Heston and Heston-Hull-White PDE. In the direction of the underlying asset we propose a standard second-order central finite difference approximation. Due to the discontinuity occurring in the first derivative of the initial condition for European options, we do not expect to obtain a higher order than two without employing additional techniques such as smoothing, projection, etc. In order to be able to concentrate grid nodes in the region of interest, we apply a coordinate transformation of the form, given by Tavella and Randall (2000),

$$h_s(s) = (c_1 + \sinh^{-1}(\tfrac{K-s}{\alpha}))/(c_1 - c_2)$$

where

$$c_1 = \sinh^{-1}(\tfrac{s_{\min}-K}{\alpha}),$$
$$c_2 = \sinh^{-1}(\tfrac{s_{\max}-K}{\alpha}).$$

The transformation maps $[s_{\min}, s_{\max}]$ to $[0, 1]$ and clusters grid points around the strike price K, which is the region of highest interest from a perspective of practitioners. Small α-values lead to a highly non-uniform grid, while large values lead to a uniform distribution of grid nodes. In our numerical tests we use $\alpha = K/4$ and a uniform grid spacing in $[0, 1]$.

In the coordinate direction of the volatility and interest rate we first apply a linear transformation to map the finite interval $[a, b]$ to the unit interval $[-1, 1]$ via

$$h_{j,1}(w_1) = \frac{2}{b-a} w_1 + \frac{a+b}{a-b}$$

for $w_1 \in [a, b]$ and $j \in \{v, r\}$. In a second step we concentrate grid points similar to Tee and Trefethen (2006), Pindza et al. (2013) via

$$h_{j,2}(w_2) = e_j \sinh\left(\frac{1}{2}(w_2 - 1)\left(\sinh^{-1}\left(\frac{1-dj}{e_j}\right) + \sinh^{-1}\left(\frac{d_j+1}{e_j}\right)\right) + \sinh^{-1}\left(\frac{1-d_j}{e_j}\right)\right) + d_j,$$

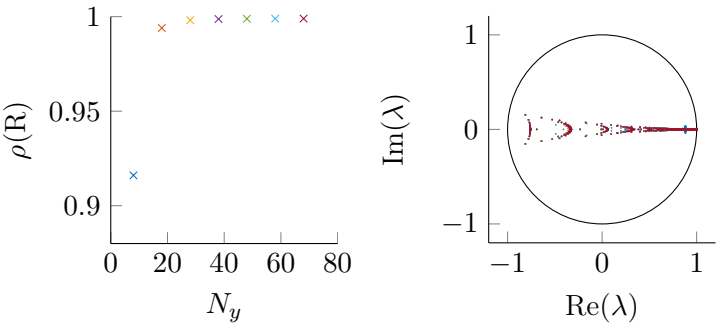

(a) DO, $\theta = 0.5$, $N_x = 100$ (b) DO, $\theta = 0.5$, $N_x = 100$

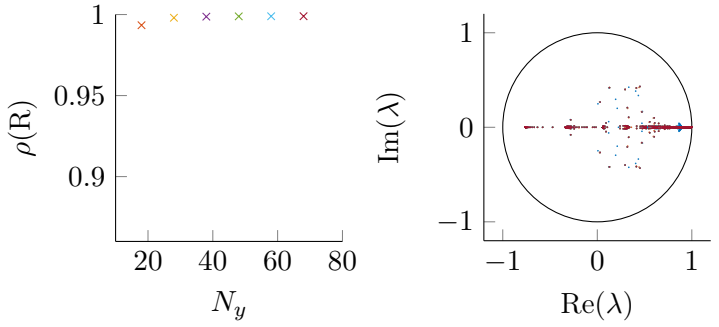

(c) CS, $\theta = 0.5$, $N_x = 100$ (d) CS, $\theta = 0.5$, $N_x = 100$

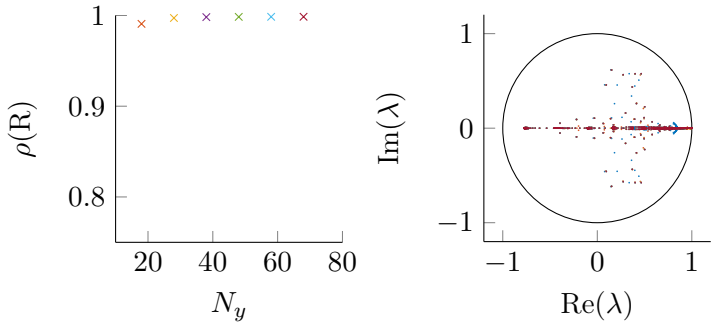

(e) MCS, $\theta = 0.42$, $N_x = 100$ (f) MCS, $\theta = 0.42$, $N_x = 100$

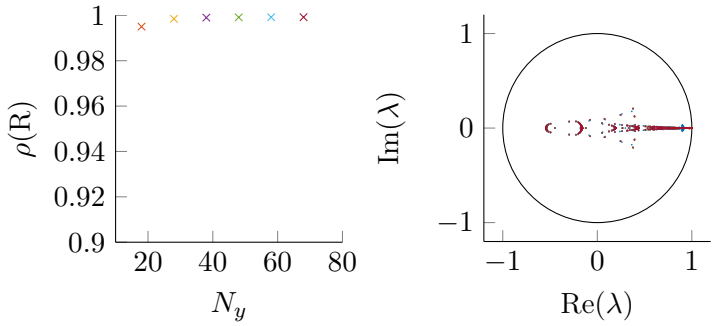

(g) HV, $\theta = 0.79$, $N_x = 100$ (h) HV, $\theta = 0.79$, $N_x = 100$

Figure 2: Dirichlet BCs at $\partial\Omega$.

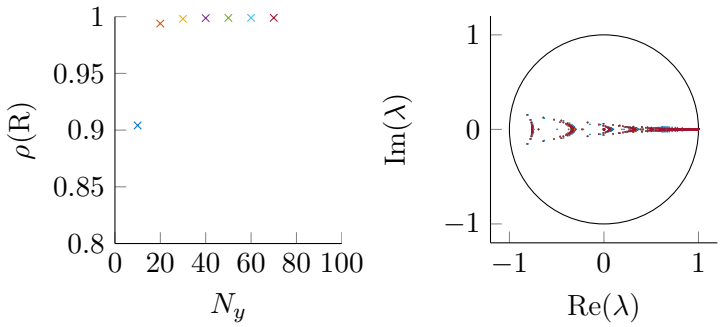

(a) DO, $\theta = 0.5$, $N_x = 100$ (b) DO, $\theta = 0.5$, $N_x = 100$

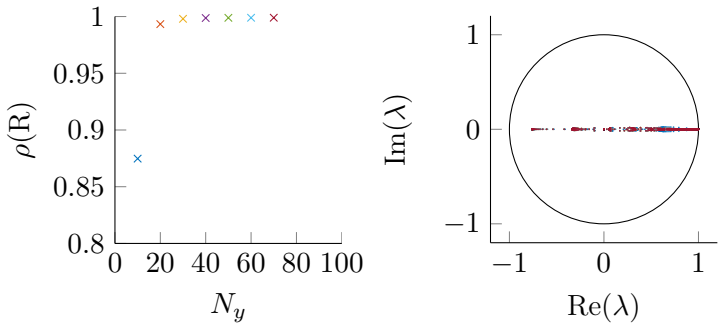

(c) CS, $\theta = 0.5$, $N_x = 100$ (d) CS, $\theta = 0.5$, $N_x = 100$

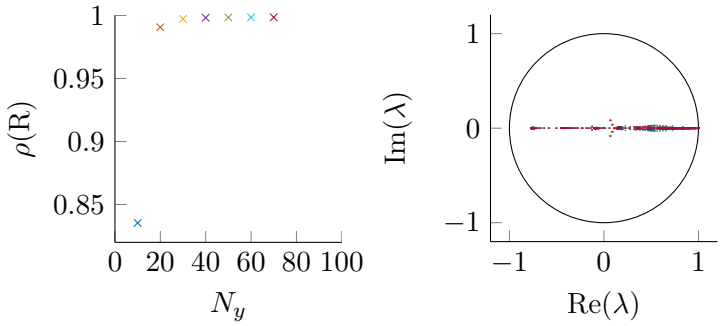

(e) MCS, $\theta = 0.42$, $N_x = 100$ (f) MCS, $\theta = 0.42$, $N_x = 100$

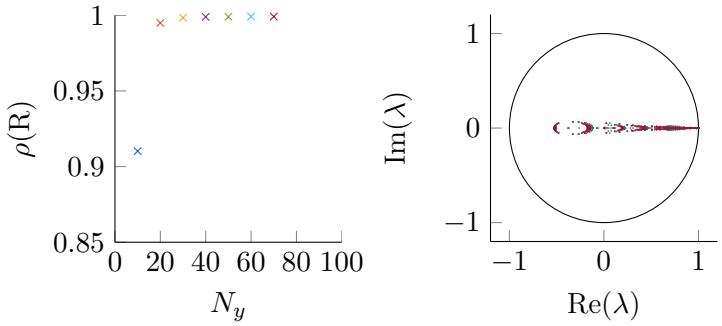

(g) HV, $\theta = 0.79$, $N_x = 100$ (h) HV, $\theta = 0.79$, $N_x = 100$

Figure 3: Neumann BCs at the boundary in y-direction, Dirichlet BCs in x.

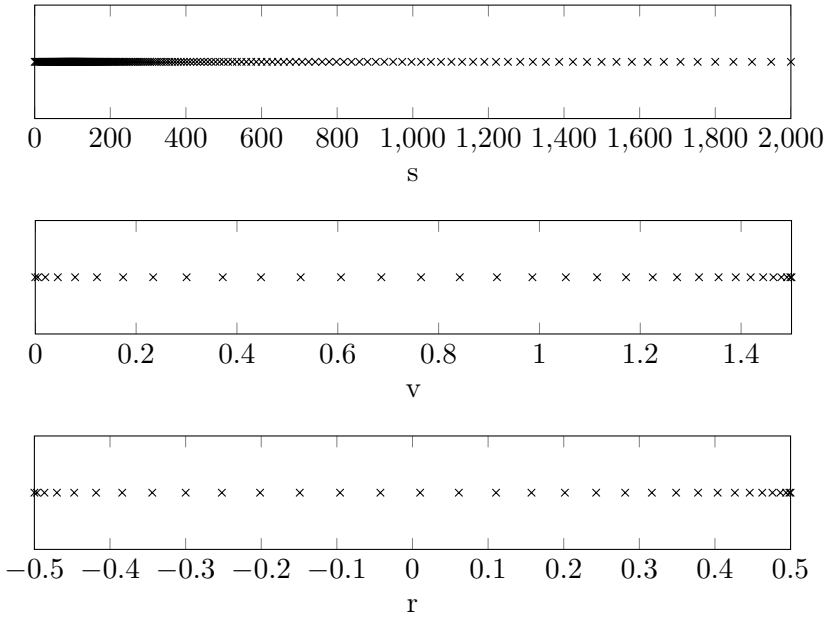

Figure 4: Sample mesh with $K = 100$, $\alpha = 25$, $e_1 = e_2 = 1$.

where the parameter $d_j \in [-1, 1]$ determines the region of clustering and $e_j > 0$ the degree of non-uniformity of the grid spacing for $j \in \{v, r\}$. The complete transformation is then given by the composition $h_j = h_{j,2} \circ h_{j,1}$. We denote the inverse of the transformations by $g_s = h_s^{-1}$, $g_j = h_j^{-1}$, respectively. Numerical tests revealed that a clustering at the upper boundary of the domain and the choice $e_1 = 10\sigma_1^2/(\kappa\eta)$ and $e_2 = 10\sigma_2^2/(a_r b_r)$ yield good results. In the numerical scheme we use a Chebyshev-Gauss-Lobatto grid in the transformed intervals $[-1, 1]$ stemming from the v and r direction, respectively. Figure 4 shows an example of the grid in the original domain.

The PDEs (1) and (2) transform to

$$\begin{aligned}\frac{\partial u}{\partial t} =& \frac{1}{2}s^2 v\left[h_s'(s)^2\frac{\partial^2 u}{\partial x^2} + h_s''(s)\frac{\partial u}{\partial x}\right] + \rho_{12}\sigma_1 s v h_s'(s)h_v'(v)\frac{\partial^2 u}{\partial x \partial y} + \frac{1}{2}\sigma_1^2 v\left[h_v'(v)^2\frac{\partial^2 u}{\partial y^2} + h_v''(v)\frac{\partial u}{\partial y}\right] \\ &+ r s h_s'(s)\frac{\partial u}{\partial x} + \kappa(\eta - v)h_v'(v)\frac{\partial u}{\partial y} - ru \end{aligned} \tag{14}$$

and

$$\begin{aligned}\frac{\partial u}{\partial t} =& \frac{1}{2}s^2 v\left[h_s'(s)^2\frac{\partial^2 u}{\partial x^2} + h_s''(s)\frac{\partial u}{\partial x}\right] + \frac{1}{2}\sigma_1^2 v\left[h_v'(v)^2\frac{\partial^2 u}{\partial y^2} + h_v''(v)\frac{\partial u}{\partial y}\right] + \frac{1}{2}\sigma_2^2\left[h_r'(r)^2\frac{\partial^2 u}{\partial z^2} + h_r''(r)\frac{\partial u}{\partial z}\right] \\ &+ \rho_{12}\sigma_1 s v h_s'(s)h_v'(v)\frac{\partial^2 u}{\partial x \partial y} + \rho_{13}\sigma_2 s\sqrt{v}h_s'(s)h_r'(r)\frac{\partial^2 u}{\partial x \partial z} + \rho_{23}\sigma_1\sigma_2\sqrt{v}h_v'(v)h_r'(r)\frac{\partial^2 u}{\partial y \partial z} \\ &+ r s h_s'(s)\frac{\partial u}{\partial x} + \kappa(\eta - v)h_v'(v)\frac{\partial u}{\partial y} + a_r(b_r - r)h_r'(r)\frac{\partial u}{\partial z} - ru, \end{aligned} \tag{15}$$

where $s = g_s(x)$, $v = g_v(y)$ and $r = g_r(z)$ with $(x, y) \in \Omega = [0, 1] \times [-1, 1]$ and $(x, y, z) \in \Omega = [0, 1] \times [-1, 1]^2$. At the boundary we impose the following conditions for the European put option under the Heston model

$$\begin{aligned} u(0, v, t) &= Ke^{-rT}, \\ u(s_{\max}, v, t) &= 0, \\ \frac{\partial u}{\partial v}(v_{\max}, s, t) &= 0, \end{aligned}$$

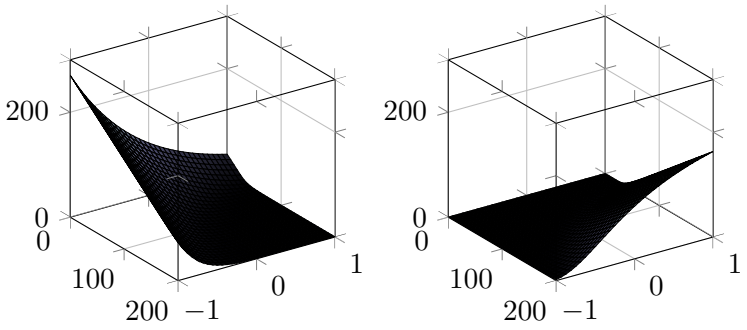

(a) European put option at $v = 0.125$ (b) European call option at $v = 0.125$

Figure 5: Reference solution of the HHW model (computed with semi closed-form pricing formula).

and under the HHW model

$$\begin{aligned} u(0, v, r, t) &= Ke^{p(r,t)}, \\ u(s_{\max}, v, r, t) &= 0, \\ \frac{\partial u}{\partial v}(s, v_{\max}, r, t) &= 0, \\ \frac{\partial u}{\partial r}(s, v, r_{\max}, tu) &= 0, \end{aligned}$$

with the discounting factor

$$\begin{aligned} p(r,t) = &-\frac{r}{a_r}\left(1 - e^{-a_r t}\right) - \frac{1}{a_r}\int_t^T b_r(1 - e^{-a_r(T-s)})ds \\ &+ \frac{\sigma_2^2}{2a_r^2}\left(t + \frac{2}{a_r}e^{-a_r t} - \frac{1}{2a_r}e^{-2a_r t} - \frac{3}{2a_r}\right). \end{aligned}$$

If the asset price is zero the option price is given by the discounted strike price. For sufficiently large s the probability that the put option ends up in-the-money tends to zero and therefore also the option value. In direction of the volatility we only imply a homogeneous Neumann boundary condition at $v_{\max}$ as suggested by in't Hout and Foulon (2010). At the boundary in direction of the interest rate, we propose a homogeneous Neumann boundary condition at $r_{\max}$. One might argue that such a condition should be applied at both boundaries of r since ρ in the Black-Scholes pricing formula vanishes for extreme values of r, but the reference solution in Figure 5 indicates, that this does not hold for the HHW model.

The application of the spatial discretization of section 2 to (14), (15) yields

$$\begin{aligned} F_{Heston}\, U = &\frac{1}{2}\mathrm{diag}(S^2 h_s'(S)^2 \otimes V) D_{FD_x}^2 \otimes I_{N_y} U + \frac{1}{2}\sigma_1^2 \mathrm{diag}(e_{N_x} \otimes V h_v'(V)^2) I_{N_x} \otimes D_{SP_y}^2 U \\ &+ \rho_{12}\sigma_1 \mathrm{diag}(S h_s'(S) \otimes V h_v'(V)) D_{FD_x} \otimes D_{SP_y} U \\ &+ \big[\frac{1}{2}\mathrm{diag}(S^2 h_s''(S) \otimes V) + r\mathrm{diag}(S h_s'(S) \otimes e_{N_y})\big] D_{FD_x} \otimes I_{N_y} U \\ &+ \big[\frac{1}{2}\sigma_1^2 \mathrm{diag}(e \otimes (V h_v''(V) + \kappa(\eta - V) h_v'(V)))\big] I_{N_x} \otimes D_{SP_y} U \\ &- rU \end{aligned}$$

and

$$
\begin{aligned}
F_{HHW}\,U =& \frac{1}{2}\mathrm{diag}(S^2 h_s'(S)^2 \otimes V \otimes e_{N_z}) D^2_{FD_x} \otimes I_{N_y} \otimes I_{N_z} U \\
&+ \frac{1}{2}\sigma_1^2 \mathrm{diag}(e_{N_x} \otimes V h_v'(V)^2 \otimes e_{N_z}) I_{N_x} \otimes D^2_{SP_y} \otimes I_{N_z} U \\
&+ \frac{1}{2}\sigma_2^2 \mathrm{diag}(e_{N_x} \otimes e_{N_y} \otimes h_r'(R)^2) I_{N_x} \otimes I_{N_y} \otimes D^2_{SP_z} \\
&+ \rho_{12}\sigma_1 \mathrm{diag}(S h_s'(S) \otimes V h_v'(V) \otimes e_{N_z}) D_{FD_x} \otimes D_{SP_y} \otimes I_{N_z} U \\
&+ \rho_{13}\sigma_2 \mathrm{diag}(S h_s'(S) \otimes \sqrt{V} \otimes h_r'(r)) D_{FD_x} \otimes I_{N_y} \otimes D_{SP_z} U \\
&+ \rho_{23}\sigma_1\sigma_2 \mathrm{diag}(e_{N_x} \otimes \sqrt{V} h_v'(V) \otimes h_r'(R)) I_{N_x} \otimes D_{SP_y} \otimes D_{SP_z} U \\
&+ \big[\frac{1}{2}\mathrm{diag}(S^2 h_s''(S) \otimes V \otimes e_{N_z}) + \mathrm{diag}(S h_s'(S) \otimes e_{N_y} \otimes R)\big] D_{FD_x} \otimes I_{N_y} \otimes I_{N_z} U \\
&+ \big[\mathrm{diag}(e_{N_x} \otimes (\frac{1}{2}\sigma_1^2 V h_v''(V) + \kappa(\eta - V) h_v'(V)) \otimes e_{N_z})\big] I_{N_x} \otimes D_{SP_y} \otimes I_{N_z} U \\
&+ \big[\mathrm{diag}(e_{N_x} \otimes e_{N_y} \otimes (\frac{1}{2}\sigma_2^2 h_r''(R) + a_r(b_r - R) h_r'(R)))\big] I_{N_x} \otimes I_{N_y} \otimes D_{SP_z} U \\
&- \mathrm{diag}(e_{N_x} \otimes e_{N_y} \otimes R)\, U,
\end{aligned}
$$

where diag is a diagonal matrix and each operation in the diag operator is understood component-wise. $e_N = (1, 1, \ldots, 1)^\top$ denotes the all-one vector of size N in x direction and of size $N+1$ in y and z direction. The spatial grid vector in s direction is given by $S \in \mathbb{R}^{N_x}$, while $V \in \mathbb{R}^{N_y+1}$ and $R \in \mathbb{R}^{N_z+1}$ are the grid vectors in the v, r direction, respectively.

The spatial discretization is now decomposed into one dimensional problems according to the ADI splitting: F_1 takes all terms, which only stem from the x direction, F_2 all terms from the y- and F_3 all terms from the z-direction. The reaction term is distributed equally over the operators F_i for $i = 1, 2, 3$. The mixed derivative terms are collected in F_0. The arising linear equation system can be solved with the help of a LU decomposition in the startup phase if the coefficients of the PDEs (1) and (2) do not depend on time. In each time step the major computational effort then consists of performing one forward and backward substitution for each leg of the ADI scheme.

In order to evaluate the performance of the scheme, we compare it to a scheme using second-order finite differences in all coordinate directions given in the articles by in't Hout and Foulon (2010), Haentjens and in't Hout (2012), but with a transformed coordinate system instead of a non-uniform grid. The following transformation is employed in the benchmark method

$$h_j(w) = \sinh^{-1}(d_j^{-1}(w - c_j)),$$

with the critical point c_j and the strength of smoothing determined by d_j for $j \in \{v, r\}$. According to in't Hout and Foulon (2010), Haentjens and in't Hout (2012) we use $c_v = 0$, $c_r = b_r$, $d_v = v_{\max}/500$ and $d_r = r_{\max}/500$.

5 Numerical results

In this section we test the hybrid method and compare it to a standard second-order finite difference discretization. In order to gain realistic performance results we consider four different scenarios given in Table 1. The parameters for the Heston model stem from in't Hout and Foulon (2010). The additional parameters for the Heston-Hull-White model have been taken from Spanderen (2011) in the case of scenario one and the parameters in the

	Case 1	Case 2	Case 3	Case 4
K	100	100	100	100
T	1	1	3	0.5
σ_1	0.3	0.04	0.2928	0.5
ρ_{12}	-0.9	0.6	-0.7571	-0.5
κ	1.5	3	0.6067	2
η	0.04	0.12	0.0707	0.02
r	0.025	0.04	0.03	0.01
a_r	0.00883	0.2	0.05	0.15
b_r	0.025	0.05	0.055	0.101
σ_2	0.00631	0.06	0.03	0.1
ρ_{13}	0.6	0.2	0.6	-0.3
ρ_{23}	-0.7	0.4	-0.2	0.2

Table 1: Scenarios for numerical tests.

scenarios two and three are taken from Haentjens and in't Hout (2012). In scenario four we have chosen the parameters in such a way that the Feller condition $2\kappa\eta > \sigma_1^2$ is violated.

We investigate both the accuracy in the time domain as well as the spatial error. Therefore, we compute

$$\mathrm{err}(\Delta_t, N) = \max|u_{\mathrm{ref}} - u_N^{\Delta_t}|,$$

where u_{ref} denotes the reference solution and $u_N^{\Delta_t}$ its approximation on the discrete grid with time step Δ_t and $N = (N_x, N_y)$ and $N = (N_x, N_y, N_z)$, respectively, grid nodes in the spatial domain. The error is always computed at the final time slice. For the sake of simplicity and to streamline our notation we choose $N_y = N_z$ in all numerical experiments and write $N = (N_x, N_y)$ instead of $N = (N_x, N_y, N_z)$. The numerical solution is computed on a grid of size $[0, 20K] \times [0, 1.5] \times [-0.5, 0.5]$ while the error is computed in the region of interest, which is defined as $[0, 2K] \times [0, 1] \times [0, 0.125]$. This choice ensures that the error due to the domain truncation in the asset direction and the error stemming from the homogeneous Neumann boundary conditions is negligible small and one does not observe any saturation effects in the numerical convergence plots. All computations have been performed on our test machine with a Intel® Core i5-4670 CPU and 20GB physical memory. The implementation of the methods has been done in Matlab®. The hybrid HHW (Heston) CS method takes about 0.10 (0.015), 0.71 (0.05), 4.65 (0.24), 85 (1.9) seconds for the following number of grid points and time steps $N = (65, 9), T/\Delta_t = 25, N = (129, 13), T/\Delta_t = 50, N = (257, 17), T/\Delta_t = 100, N = (512, 33), T/\Delta_t = 100$, respectively, to compute the solution. The MCS and HV scheme have approximately the same runtime, while the Douglas method just has one implicit sweep and therefore the computation takes about half of the runtime.

In our first numerical experiment we investigate the error decay for $\Delta_t \to 0$. Here the reference solution is given by a highly accurate numerical approximation $u_{\mathrm{ref}} := u_N^{2^{-13}}$ with $N = (129, 33)$ nodes. The θ value within the ADI procedure is always chosen according to the lowest possible value ensuring unconditional stability, given in section 3, see Table 2. Please note, that we choose $\theta = 0.34$ in case of the MCS scheme for the Heston model as it holds for the correlations $|\rho| \leq 0.96$ for all test scenarios. Although these bounds have been derived for finite difference schemes in the von Neumann framework, the positive results of section 3.1 encourage that these are also valid for the Chebyshev spectral method. Figures 6 and 8 show that the error decays monotonically both for the Heston and the

	DO	CS	MCS	HV
Heston	0.5	0.5	0.34	0.79
HHW	0.67	0.5	$\max\{\frac{1}{3}, \frac{2}{13}(2\gamma+1)\}$	0.79

Table 2: θ-values used in the ADI methods within the numerical experiments, where $\gamma = \max\{|\rho_{12}|, |\rho_{13}|, |\rho_{23}|\}$.

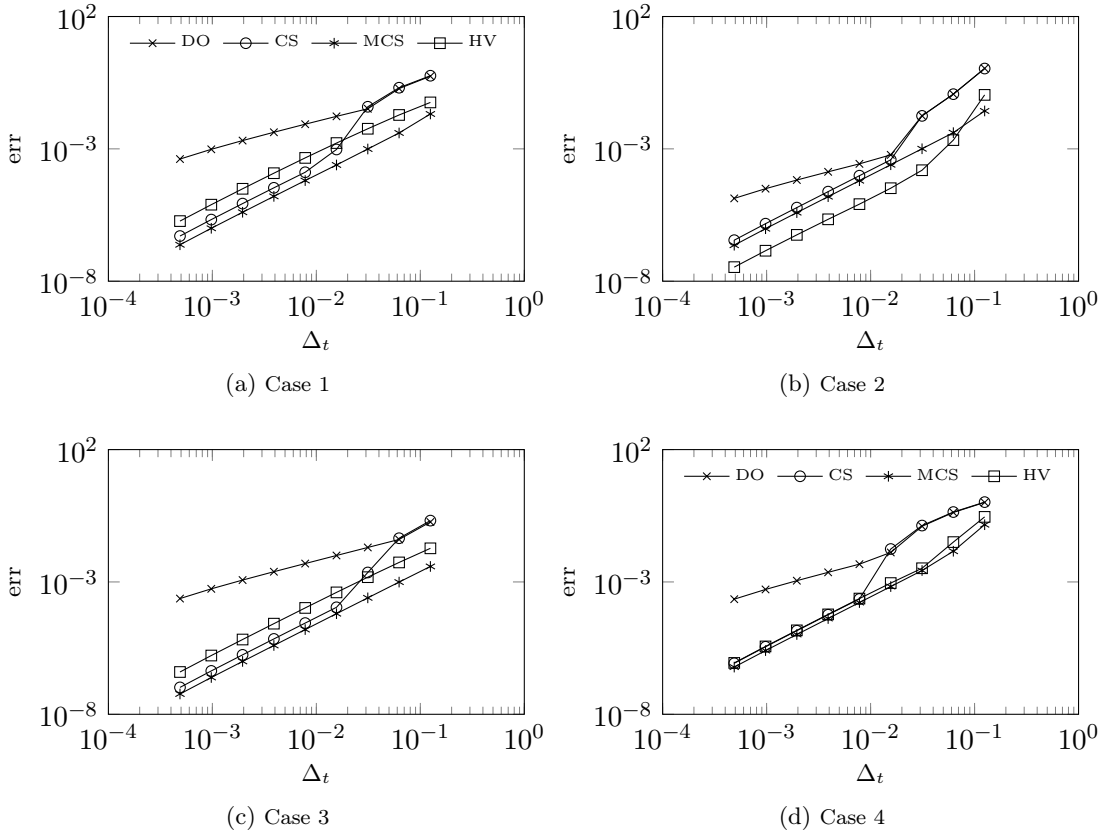

(a) Case 1

(b) Case 2

(c) Case 3

(d) Case 4

Figure 6: Heston: convergence in time. 129 grid points in S- and 33 in v-direction.

HHW model. The DO scheme exhibits order one, while the error of the CS, MCS and HV scheme decreases with second-order. If the time step Δ_t is very large the schemes show an undesirable high error. Especially the DO and CS scheme suffer from a large error in all four test scenarios. In order to improve the results we employ a kind of Rannacher startup (Giles and Carter (2006)) and perform four steps with $\Delta_t/4$ and $\theta = 1$ to damp high frequency errors, which arise due to the non-smooth initial condition. The Figures 7 and 9 show that the startup procedure is capable to smooth the error and thus leads to a much smaller error for large time steps.

For the experiments in the spatial domain we use the semi closed-form solution to the Heston and Heston-Hull-White PDE from Heston (1993), in't Hout et al. (2007). In the case of the Heston-Hull-White model the pricing formula is available under the assumption that $\rho_{13} = \rho_{23} = 0$. Hence, we set these correlation values to zero in the following numerical experiments. It is well known that the complex logarithm in the pricing formula faces discontinuities and we therefore follow the approach by Kahl and Jäckel (2005) and apply a rotation count correction algorithm to both pricing formulas. The experiments are performed with the CS ADI scheme with $\theta = 0.5$. The other schemes have the same spatial discretization and thus lead to the same results except for roundoff errors.

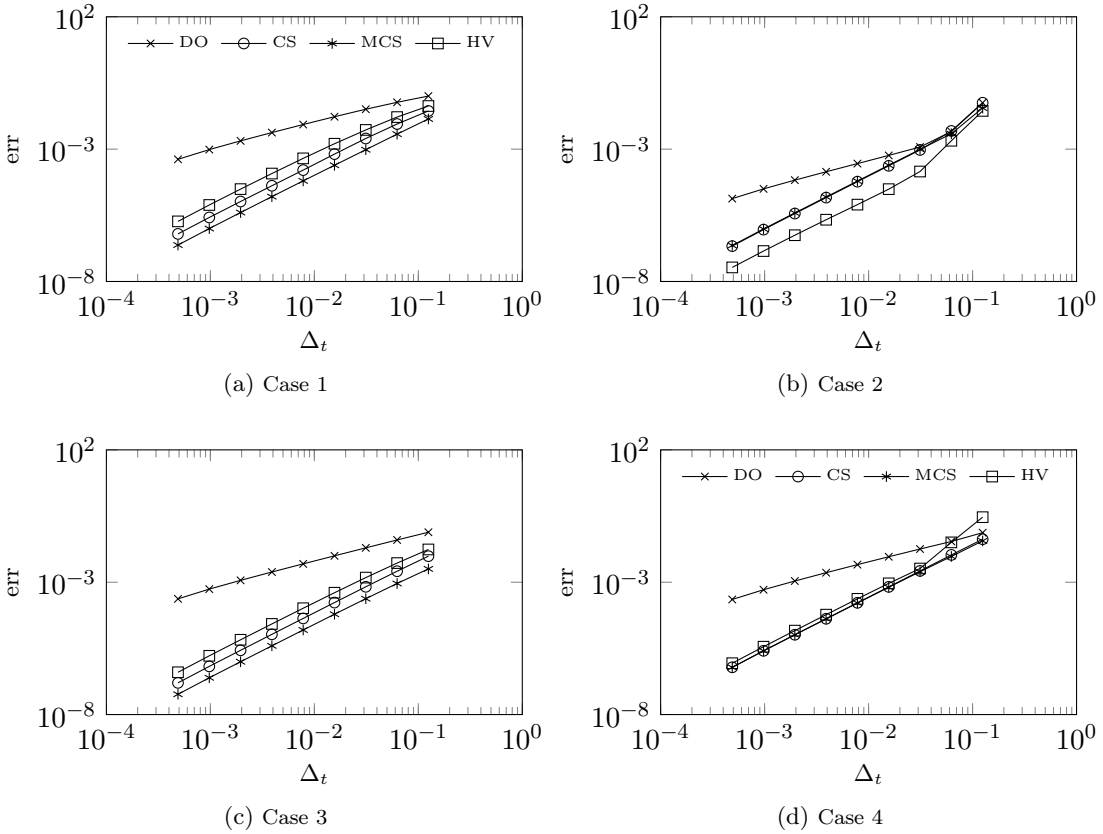

(a) Case 1 (b) Case 2

(c) Case 3 (d) Case 4

Figure 7: Heston: convergence in time with four initial steps using $\theta = 1$. 129 grid points in S- and 33 in v-direction.

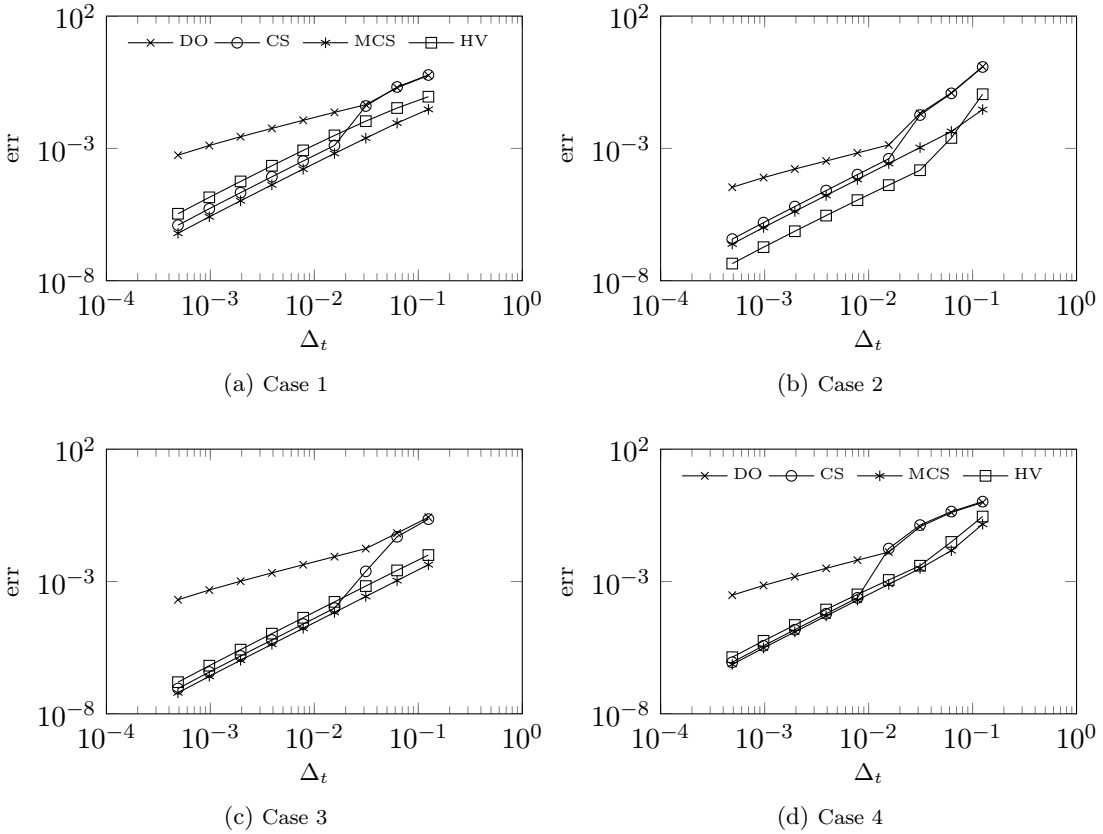

(a) Case 1 (b) Case 2

(c) Case 3 (d) Case 4

Figure 8: Heston-Hull-White: convergence in time. 129 grid points in S- and 33 in v- and r-direction.

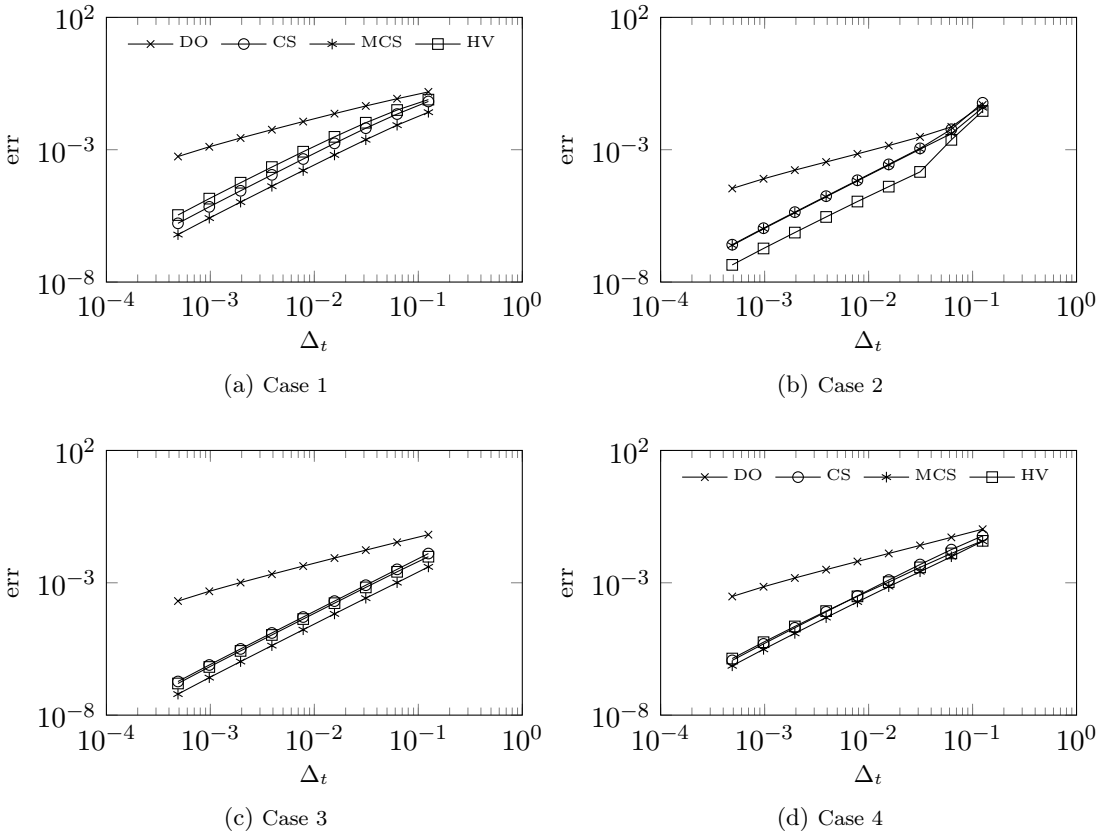

(a) Case 1 (b) Case 2

(c) Case 3 (d) Case 4

Figure 9: Heston-Hull-White: convergence in time with four initial steps using $\theta = 1$. 129 grid points in S- and 33 in v- and r-direction.

Figures 10 and 11 show the convergence in the direction of the underlying asset. In order to ensure that the error stemming from the first coordinate direction is dominant, we place 45 grid points in the direction of volatility, interest rate, respectively. This choice leads to negligible small errors in v and r. In the time discretization we use $\Delta_t = 10^{-3}$. We observe an error decay with the desired order close to two.

In Figure 12 and 13 we compare the convergence of the spectral approximation to the second-order finite difference approximation. The plots reveal that the spectral accuracy allows to use significantly less grid points than in the finite difference discretization to achieve the same accuracy, but at the cost of densely filled discretization matrices. Thus, it is of highest interest if the spectral accuracy can offset this drawback. Let N_{SP} denote the number of grid points in each direction of the Chebyshev discretization and N_{FD} the number of nodes for the finite difference scheme in direction v and/or r. Please note, that we neglect the influence of discretization of the asset direction in the following discussion. As it can be seen from Figure 16 (a) the computational effort of the ADI scheme for the Chebyshev and FD discretization for the Heston model grow with $\mathcal{O}(N_{SP}^2)$ and $\mathcal{O}(N_{FD})$. Both approaches have the same run-time if $N_{SP}^2 \approx 5N_{FD}$. As mentioned before, the major workload consists of performing a forward and backward substitution to solve the linear equation system in each leg of the ADI scheme after the LU decomposition has been computed during a startup phase. For a full quadratic matrix of size N this consists of N^2 operations compared to $2N$ operations for the forward and $3N$ operations for the backward substitution in case of a tridiagonal matrix. Thus, the run-time for both methods is equivalent if $N_{SP}^2 \approx 5N_{FD}$. In the three dimensional case of the HHW model $N_x \cdot N_{SP}$ one dimensional problems have to be solved with an effort of $\mathcal{O}(N_{SP}^2)$ and thus the runtime

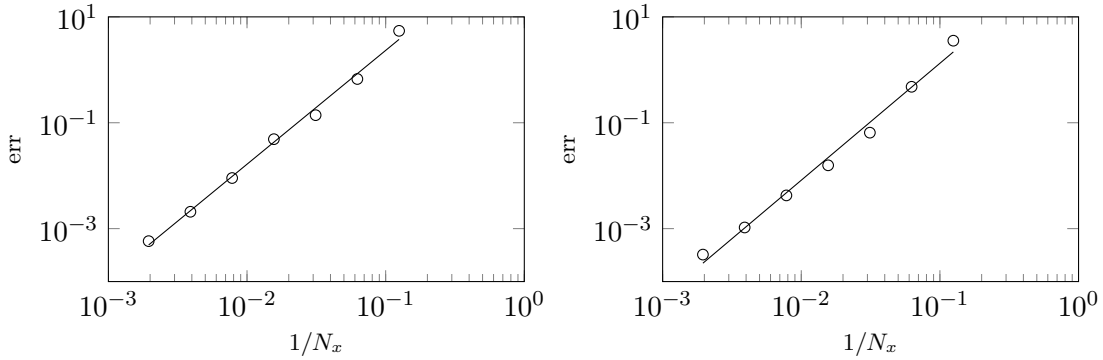

(a) Case 1, slope 2.15

(b) Case 2, slope 2.19

(c) Case 3, slope 2.25

(d) Case 4, slope 2.06

Figure 10: Heston: convergence in space with dominating stock direction error (hybrid CS ADI scheme), $N_y = 45$.

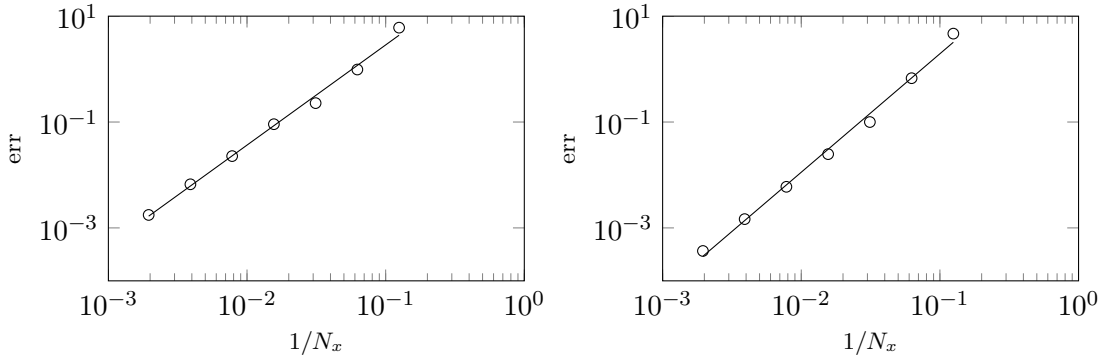

(a) Case 1, slope 1.84

(b) Case 2, slope 2.24

(c) Case 3, slope 2.11

(d) Case 4, slope 2.20

Figure 11: Heston-Hull-White: convergence in space with dominating stock direction error (hybrid CS ADI scheme), $N_y = N_z = 45$.

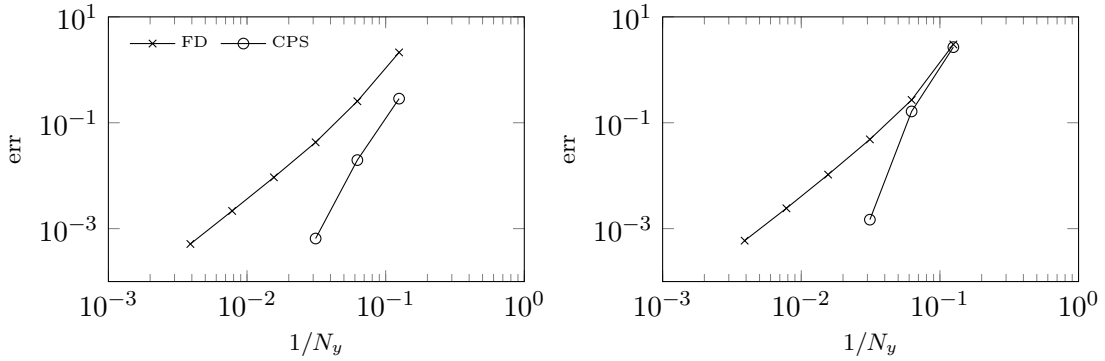

(a) Case 1 (b) Case 2

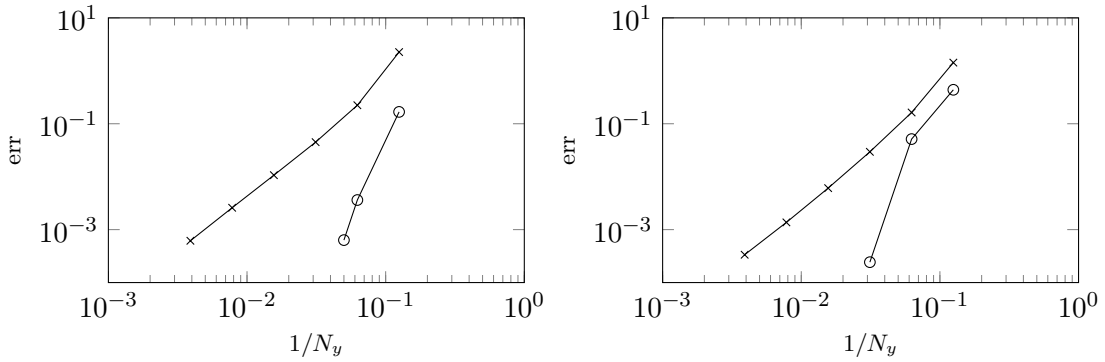

(c) Case 3 (d) Case 4

Figure 12: Heston: convergence in direction of volatility with 1025 grid nodes in direction of the asset and $\Delta_t = 10^{-3}$.

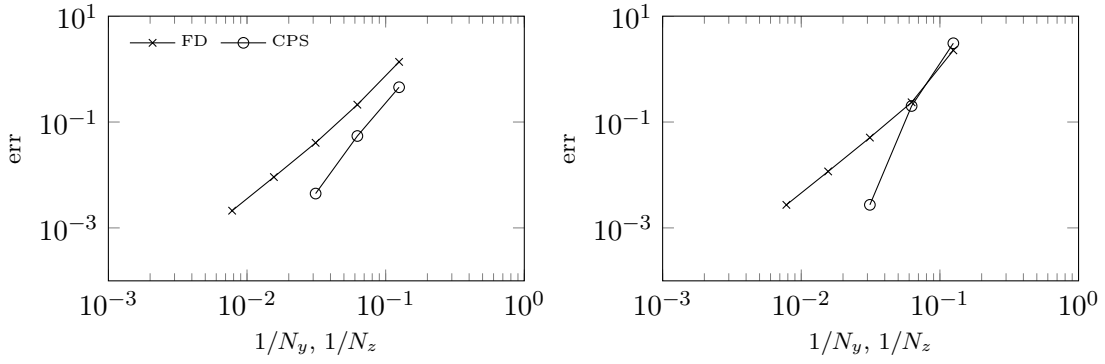

(a) Case 1 (b) Case 2

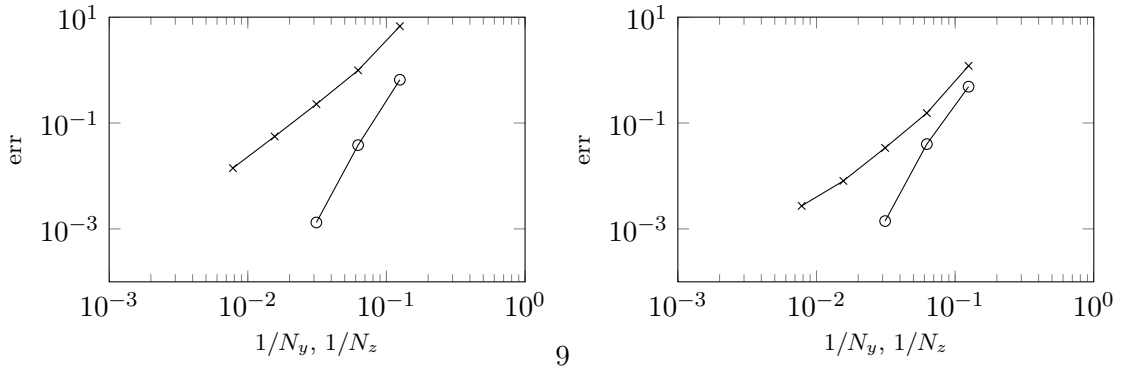

(c) Case 3 (d) Case 4

Figure 13: Heston-Hull-White: convergence in direction of volatility/interest rate with 513 grid nodes in direction of the asset and $\Delta_t = 10^{-3}$.

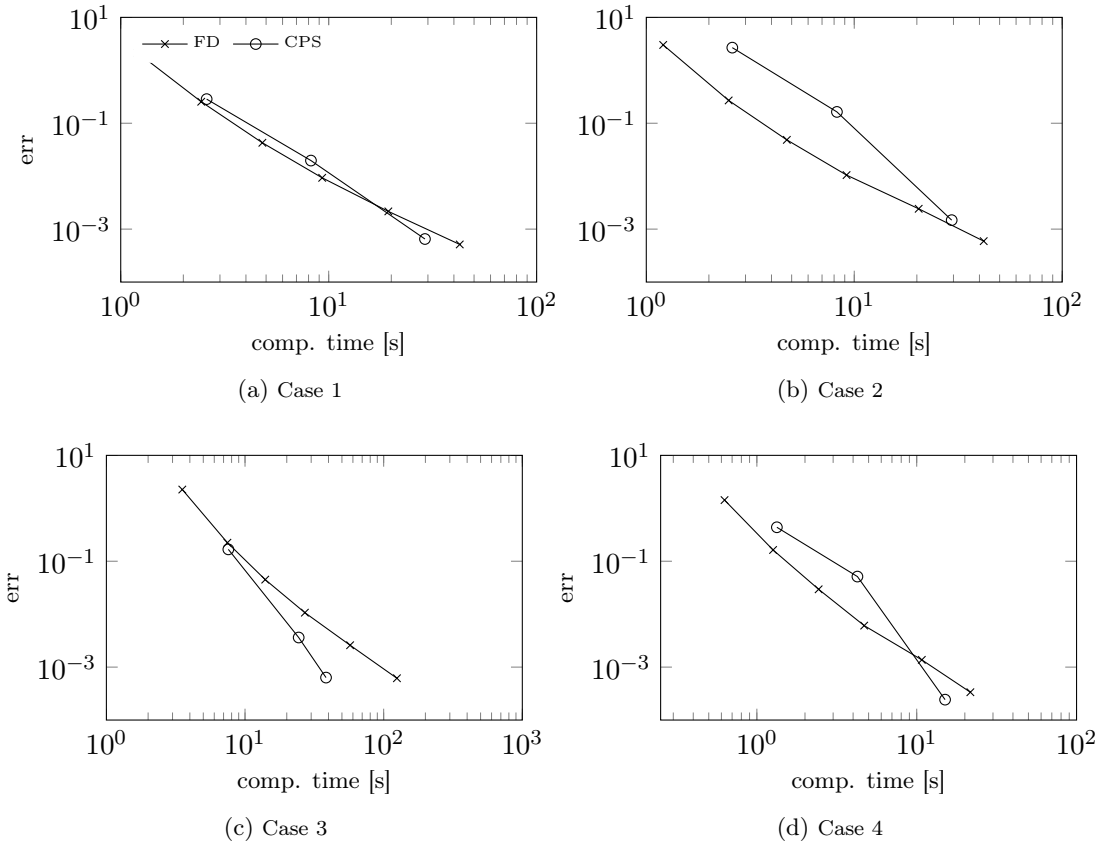

(a) Case 1 (b) Case 2

(c) Case 3 (d) Case 4

Figure 14: Heston: accuracy versus computation time in direction of volatility with 1025 grid nodes in direction of the asset and $\Delta_t = 10^{-3}$.

grows with $\mathcal{O}(N_{SP}^3)$. The analogue arguments lead to a growth of $\mathcal{O}(N_{FD}^2)$ for the FD discretization. Figure 16 (b) underlines this result and we see a slope of 3.06 (excluding first two data points), 2.03 respectively. Both methods have the same run-time if $N_{SP}^3 \approx 5N_{FD}^2$. In the general d dimensional case, under the assumption that the solution is sufficiently smooth in $d-1$ coordinate direction, such that $d-1$ Chebyshev approximations can be applied, we expect a growth of $\mathcal{O}(N_{SP}^d)$, while we expect one of $\mathcal{O}(N_{FD}^{d-1})$ for the FD method. Hence, the computational effort is approximately the same if $N_{SP}^{d/(d-1)} 1/5^{1/(d-1)} \approx N_{FD}$ holds. As the left hand side is monotonically decreasing for growing d the hybrid FD/SP approach with ADI time splitting becomes more efficient compared to the FD discretization for higher dimensional problems. The dashed line in Figure 16 underlines that the theoretical result $N_{SP}^{d/(d-1)} 1/5^{1/(d-1)} \approx N_{FD}$ holds in practice. Please note, that the explicit treatment of the mixed derivative term $\frac{\partial^2 u}{\partial y \partial z}$ in (15) via matrix-vector multiplication has a computational effort proportional to $\mathcal{O}(N_{SP}^4)$ since both Chebyshev differentiation matrices are full. Hence, we perform the Chebyshev differentiation via a Fast-Fourier-Transform (FFT) to reduce the complexity for each differentiation to $\mathcal{O}(\log(N_{SP})N_{SP})$. For more details regarding this technique we refer to Trefethen (2000). The computation of the mixed term can then be performed by applying the FFT algorithm twice (y-, z-direction), which leads to $\mathcal{O}(\log^2(N_{SP})N_{SP}^2)$ operations. In contrast, with central second-order finite differences the derivative can be computed in linear runtime due to the sparse structure (≤ 4 entries per row) of the discretization matrix.

Figure 14 and 15 show the accuracy versus computation time. The hybrid method is able to outperform the FD method in the majority of the test scenarios - only in case two of the Heston model, the FD method yields more accurate result. In the three dimensional

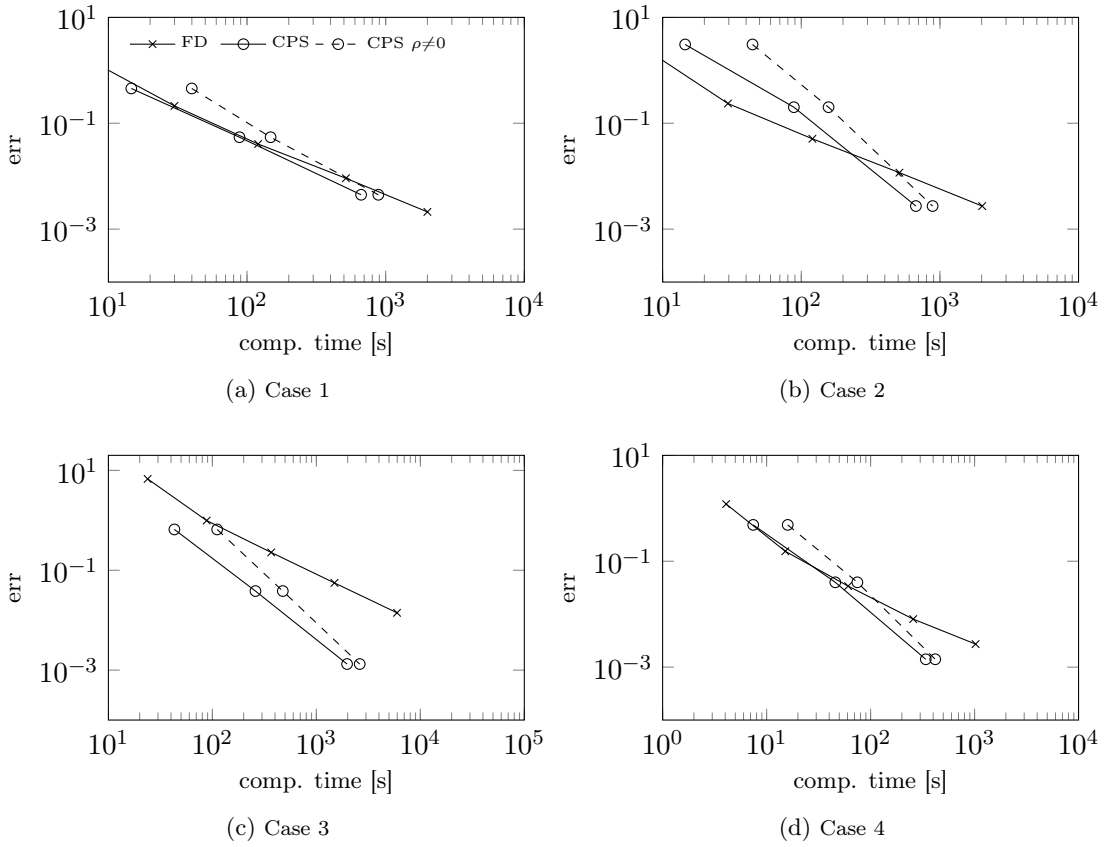

(a) Case 1 (b) Case 2

(c) Case 3 (d) Case 4

Figure 15: Heston-Hull-White: accuracy versus computation time in direction of volatility/interest rate with 513 grid nodes in direction of the asset and $\Delta_t = 10^{-3}$.

case of the HHW model the spectral discretization achieves a higher accuracy than the FD scheme even for small run-times in test cases 1,3,4 and even in case 2 the method is able to beat its benchmark in the high accuracy region. These results can be explained by the argumentation given above. The geometric error decay of the Chebyshev approximation in combination with ADI time stepping shows its strength if highly accurate results for higher dimensional problems are desired. Here, the fast convergence compensates the disadvantage of full discretization matrices and the second-order FD discretization is clearly outperformed. The dashed lines in Figure 15 show the runtime if $\rho_{13} \neq 0$, $\rho_{23} \neq 0$. Since in this case no reference solution is available, we are content with the error of the uncorrelated case ($\rho_{13} = \rho_{23} = 0$). For the sake of readability we omit to plot the runtime for non-zero correlation in case of the pure finite difference method as the runtime does not change very much.

In an additional experiment we investigate the runtime properties for time-dependent parameters. Therefore, we consider a time-dependent long term mean in direction of the interest rate within the HHW model. Similar to Haentjens and in't Hout (2012) we use

$$b_r(t) = c_0 - c_1 e^{-c_2 \cdot (t)},$$

with constants c_0, c_1 and c_2. The third implicit leg in the ADI schemes changes to

$$Y_3 = Y_2 + \theta \Delta_t \big(F_3((n+1)\Delta_t) Y_3 - F_3(n\Delta_t) \big) U_n$$

and the computation of $\tilde{Y}_3$ has to be modified in an analogue way. In the explicit steps F, F_0 depend on point in time $n\Delta_t$. Due to the time dependency the implicit system to

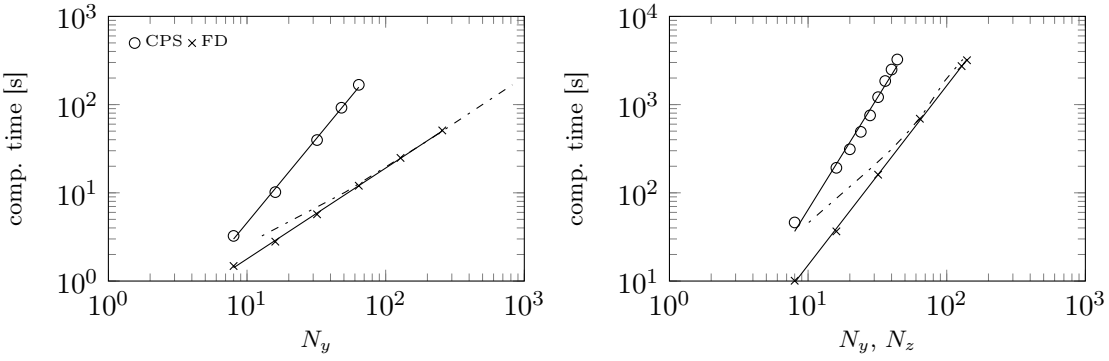

(a) Heston: slope SP 1.91, slope FD 1.03.

(b) Heston-Hull-White: slope SP 3.06 (excluding first two data points), slope FD 2.03.

Figure 16: Heston and HHW run-time scaling for growing number of grid nodes in v and r direction with fixed number of grid nodes in the asset direction (Heston: $N_x = 1025$, correlation $\neq 0$, HHW: $N_x = 513$, all correlations $\neq 0$, $\frac{\partial^2 u}{\partial y \partial z}$ via FFT differentiation) and 1000 time steps. The dotted line shows the shifted Chebyshev run-time curve: $N_{SP}^{d/(d-1)} 1/5^{1/(d-1)}$ for $d = 2$, $d = 3$ respectively.

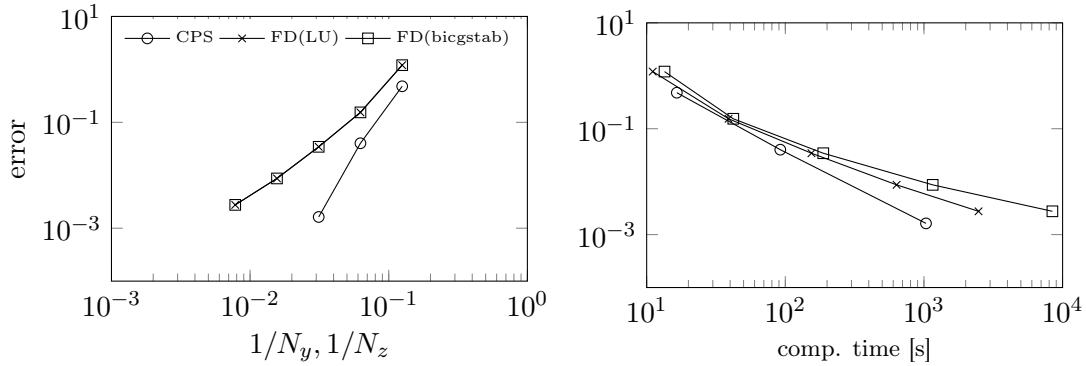

(a) N_y, N_z vs. error.

(b) Comp. time vs. error.

Figure 17: HHW: accuracy in direction of volatility/interest rate with 513 grid nodes in direction of the asset, $\rho_{13} = \rho_{23} = 0$, $\Delta_t = 10^{-3}$ and time dependent parameter b_r.

compute Y_3, $\tilde{Y}_3$ has to be solved in each time iteration and cannot be solved via a LU decomposition in a startup phase. If the system is solved by a direct method this leads to an complexity of $N_{SP} \cdot \mathcal{O}(N_{SP}^3) = \mathcal{O}(N_{SP}^4)$, whereas the complexity for the pure finite difference scheme remains $N_{FD} \cdot \mathcal{O}(N_{FD}) = \mathcal{O}(N_{FD}^2)$. In order to reduce the computational effort we employ an iterative solver. For our numerical example we choose the Matlab® builtin solver *bicgstab* with an effort of $\mathcal{O}(N^2)$ per iteration for a quadratic matrix of size N. Thus, if the number of iterations is small, one can apply similar arguments like in the previous analysis to show that both methods have approximately the same runtime if $\mathcal{O}(N_{SP}^{d/(d-1)}) = \mathcal{O}(N_{FD})$ is fulfilled. In Figure 17 we compare the run-time of the hybrid to the finite difference method with the parameters of scenario 4 and $c_0 = 0.101$, $c_1 = 0.003$, $c_3 = 1$. As the starting value for the iterative solver we use the solution of the previous leg Y_2, $\tilde{Y}_2$, respectively. For this choice the solver convergences in less than three iterations in our experiment. Similar to the time-independent case the Chebyshev method is able to outperform the benchmark method. The sparse linear equation system within the finite difference method can be solved very efficiently and hence it is not necessary to use an iterative solver. In our numerical experiment this even led to a longer computation time.

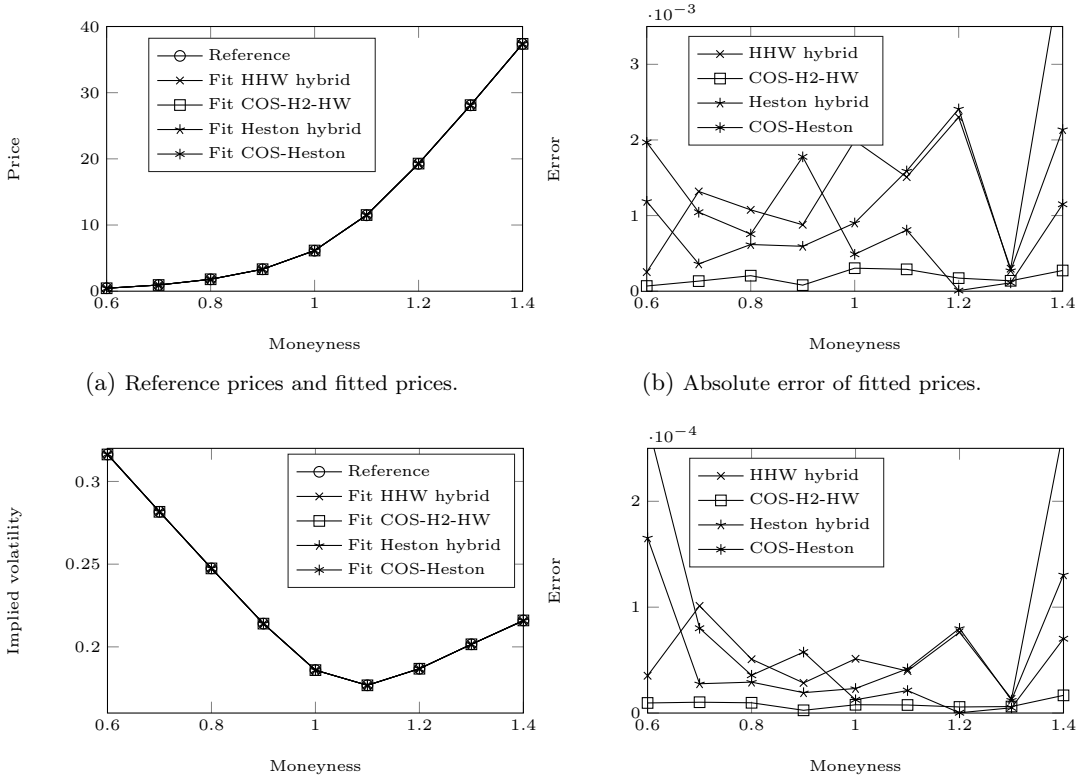

(a) Reference prices and fitted prices.

(b) Absolute error of fitted prices.

(c) Reference Black-Scholes implied volatilities and fitted volatilities.

(d) Absolute error of fitted Black-Scholes volatilities.

Figure 18: Calibration results to synthetic data with $\rho_{13} = 0.4$, $\rho_{23} = 0$ and $T = 1$.

5.1 Calibration

In this paragraph we evaluate the robustness of the hybrid method in a calibration setting. Therefore, we use synthetic data and compute reference option prices with the COS method, given by Fang and Oosterlee (2008). In order to compute the characteristic function we employ the H2-HW approximation derived by Grzelak and Oosterlee (2011). We use a fixed correlation of $\rho_{13} = 0.4$. The calibration is performed in two steps: first we fit the interest rate parameters and in a second step we calibrate the remaining parameters. In the fitting procedure we minimize the Mean-Square-Error (MSE) of the option prices using the Matlab® routine *fmincon* with the starting vector $(\sigma_1, \kappa, \eta, v_0, \rho_{12}) = (0.5, 1, .0.5, 0.02, 0)$. The interest rate parameters are $a_r = 0.4$, $b_r = 0.025$ and $\sigma_2 = 0.01$ and $r_0 = 0.025$. Table 3 shows the calibration results of the COS and the hybrid method for the Heston and HHW model. All methods achieve an accurate fit to the data. The COS-H2-HW method shows the lowest MSE, but since this method has been used to produce the synthetic data, this superior result is not surprising. The COS method and the hybrid method give quite similar parameter fits. Only the κ value for the Heston model shows a notable difference. In Figure 18 the fitted prices and implied volatilities are compared. The hybrid approach provides satisfactory accurate prices and implied volatilities, which underlines the robustness of our proposed numerical method.

method	κ	η	σ_1	v_0	ρ_{12}	MSE
Heston hybrid	0.2741	0.0626	0.6019	0.0487	-0.2931	1.7854(e-06)
COS-Heston	0.3104	0.0538	0.6067	0.0500	-0.2910	1.2124(e-06)
HHW hybrid	0.2456	0.0618	0.5957	0.0483	-0.2951	3.8354(e-06)
COS-H2-HW	0.2494	0.0672	0.5963	0.0478	-0.3007	4.1179(e-08)

Table 3: Calibrated model parameters for synthetic data with $\rho_{13} = 0.4$, $\rho_{23} = 0$ and $T = 1$.

6 Conclusion

In this article we have introduced a hybrid FD / CSP method for two and three factor models. As a testbed we have considered the Heston and HHW PDEs. The numerical eigenvalue analysis in the case of Dirichlet and Neumann boundary conditions indicated that the spatial approximation in combination with ADI time marching is unconditionally stable if θ fulfills the bounds, which were derived for FD schemes in the von Neumann framework. The error of the two and three dimensional method decayed monotonically in all numerical test cases with the desired order of convergence. Thus, the usage of spectral methods has no negative impact on the stability properties of the ADI method. The undesirable large error for small time steps could successfully be removed by a variant of Rannacher time stepping with four initial steps with $\Delta_t/4$ and $\theta = 1$. In the spatial domain we compared the hybrid FD/ CSP method to a pure FD method. Although the discretization matrices are full in the spectral case, the computational effort could be decreased by decomposing the arising linear system into a sequence of one dimensional problems. The effort for both approaches turned out to be approximately equivalent if $\mathcal{O}(N_{SP}^{d/(d-1)}) = \mathcal{O}(N_{FD})$ holds. Thus, the difference in the computational complexity between the CSP and FD method becomes smaller if the number of spatial dimensions grows. This theoretical results could be validated in numerical experiments and especially in the three dimensional case the hybrid method showed a significant better performance.

At the current state the low rate of convergence in the asset direction is a major bottleneck. In a forthcoming paper we plan to apply a high-order-compact finite difference discretization to increase the order of accuracy. These kind of discretizations allow to compute a fourth order accurate solution on the compact stencil. Further, we want to investigate the behavior of the hybrid method for American option pricing problems. Here the free boundary value problem could be solved via penalty methods (Zvan et al. (1998)) or via the partial differential complementarity problem (Haentjens and in t Hout (2015)). Alternatively the free boundary can be tracked exactly as suggested by Han and Wu (2003).

Acknowledgement

The work of the authors was partially supported by the European Union in the FP7-PEOPLE-2012-ITN Programme under Grant Agreement Number 304617 (FP7 Marie Curie Action, Project Multi-ITN STRIKE – Novel Methods in Computational Finance).
Further the authors acknowledge partial support from the bilateral German-Spanish Project HiPeCa – High Performance Calibration and Computation in Finance, Programme Acciones Conjuntas Hispano-Alemanas financed by DAAD.

References

F. Black and M. Scholes. The pricing of options and corporate liabilities. *J. Polit. Econ.*, 81:637–659, 1973.

M. Briani, L. Caramellino, and A. Zanette. A hybrid approach for the implementation of the Heston model. *IMA J. of Manag. Math.*, 2015. doi: 10.1093/imaman/dpv032. URL http://imaman.oxfordjournals.org/content/early/2015/11/12/imaman.dpv032.abstract.

M Briani, L. Caramellino, and A. Zanette. A hybrid tree/finite-difference approach for Heston-Hull-White type models. *J. Comp. Fin., to appear*, 2016. doi: ArXiv:1503.03705.

C. Canuto, M.Y. Hussaini, A. Quarteroni, and T.A. Zang. *Spectral methods : fundamentals in single domains*. Scientific computation. Springer, Berlin, 2006. ISBN 3-540-30725-7. URL http://opac.inria.fr/record=b1127559.

B. Düring and M. Fournie. High-order compact finite difference scheme for option pricing in stochastic volatility models. *J. Comput. Appl. Math.*, 236(17):4462–4473, 2012. doi: 10.1016/j.cam.2012.04.017. URL http://dx.doi.org/10.1016/j.cam.2012.04.017.

B. Düring, M. Fournie, and C. Heuer. High-orderrder compact finite difference schemes for option pricing in stochastic volatility models on non-uniform grids. *J. Comput. Appl. Math.*, 271:247–266, 2014.

F. Fang and C. W. Oosterlee. A novel pricing method for European options based on Fourier-Cosine series expansions. *SIAM J. Sci. Comput.*, 31(2):826–848, November 2008. ISSN 1064-8275. doi: 10.1137/080718061. URL http://dx.doi.org/10.1137/080718061.

I. Florescu and V. Frederi. A binomial tree approach to stochastic volatility driven model of the stock price. *An. of Univ. Craiova, Math. Comp. Sci.*, 32:126–142, 2005a.

I. Florescu and V. Frederi. Stochastic volatility: option pricing using a multinomial recombining tree. *Appl. Math. Fin.*, 15(2):151–181, 2005b.

A. Gil, J. Segura, and N. Temme. *Numerical methods for special functions*. Society for Industrial and Applied Mathematics, 2007. doi: 10.1137/1.9780898717822. URL http://epubs.siam.org/doi/abs/10.1137/1.9780898717822.

M. B. Giles and R. Carter. Convergence analysis of Crank-Nicolson and Rannacher time-marching. *J. Comp. Fin.*, 9(4), 2006.

D. Gottlieb and L. Lustman. The spectrum of the Chebyshev collocation operator for the heat equation. *SIAM Journal on Numerical Analysis*, 20(5):909–921, 1983. doi: 10.1137/0720063. URL http://dx.doi.org/10.1137/0720063.

D. Gottlieb, M. Y. Hussaini, and S.A. Orszag. Theory and applications of spectral methods. In R. G. Voigt, D. Gottlieb, and M. Y. Hussaini, editors, *Spectral Methods for Partial Differential Equations*, pages 1–54, 1984.

L. A. Grzelak and C. W. Oosterlee. On the Heston model with stochastic interest rates. *SIAM Journal on Financial Mathematics*, 2(1):255–286, 2011. doi: 10.1137/090756119. URL http://dx.doi.org/10.1137/090756119.

T. Haentjens and K. J. in t Hout. ADI Schemes for pricing American options under the Heston model. *Appl. Math. Fin.*, 22(3):207–237, 2015. doi: 10.1080/1350486X.2015.1009129. URL http://dx.doi.org/10.1080/1350486X.2015.1009129.

T. Haentjens and K. J. in't Hout. ADI finite difference schemes for the Heston-Hull-White PDE. *J. Comp. Fin.*, 16:83–110, 2012.

H. Han and X. Wu. A fast numerical method for the Black–Scholes equation of American options. *SIAM J. Numer. Anal.*, 41(6):2081–2095, 2003. doi: 10.1137/S0036142901390238. URL http://dx.doi.org/10.1137/S0036142901390238.

C. Hendricks, M. Ehrhardt, and M Günther. High-order ADI schemes for diffusion equations with mixed derivatives in the combination technique. *Appl. Numer. Math.*, 101:36 – 52, 2016. ISSN 0168-9274.

S. L. Heston. A closed-Formorm solution for options with stochastic volatility with applications to bond and currency options. *The Review of Financial Studies*, 6(2):327–343, 1993.

W. Hundsdorfer. Stability of approximate factorization with θ-methods. *BIT Numer. Math.*, 39(3):473–483, 1999. ISSN 0006-3835.

K. in't Hout, J. Bierkens, A. P. C. van der Ploeg, and J. in't Panhuis. A semi closed-form analytic pricing formula for call options in a hybrid Heston–Hull–White model. *Proceedings of the 58th European Study Group Mathematics with Industry, eds. R.H. Bisseling et. al., Utrecht*, pages 101–105, 2007.

K. J. in't Hout and S. Foulon. ADI finite difference schemes for option pricing in the Heston model with correlation. *Int. J. Numer. Anal. Mod.*, 7:303–320, 2010.

K. J. in't Hout and C. Mishra. Stability of the Modified Craig-Sneyd scheme for two-dimensional convection-diffusion equations with mixed derivative terms. *Math. Comp. Simul.*, 81:2540–2548, 2011.

K. J. in't Hout and C. Mishra. Stability of ADI schemes for multidimensional diffusion equations with mixed derivative terms. *Appl. Numer. Math*, 74:83–94, 2013.

K. J. in't Hout and B. D. Welfert. Stability of ADI Schemes applied to convection-diffusion equations with mixed derivative terms. *Appl. Numer. Math.*, 57(1):19–35, January 2007. ISSN 0168-9274.

K. J. in't Hout and B.D. Welfert. Unconditional stability of second-order ADI schemes applied to multi-dimensional diffusion equations with mixed derivative terms. *Appl. Numer. Math.*, 59(3-4):677–692, 2009.

K. J. in't Hout and M. Wyns. Convergence of the Modified Craig-Sneyd scheme for two-dimensional convection-diffusion equations with mixed derivative term. *J. Comput. Appl. Math.*, 296(C):170–180, April 2016. ISSN 0377-0427.

C. Kahl and P. Jäckel. Not-so-complex logarithms in the Heston model. *Wilmott Magazine*, pages 94–103, 2005.

T. Kluge. Pricing derivatives in stochastic volatility models using the finite difference method. Master's thesis, Technische Universität Chemnitz Fakultät für Mathematik, 2002.

D. Lanser, J.G. Blom, and J.G. Verwer. Time integration of the Shallow Water equations in spherical geometry. *J. Comp. Pyhs.*, 171:373–393, 2001.

G. Linde, J. Persson, and L. Von Sydow. High-order adaptive space discretizations for the Black-Scholes equation. Master thesis, 2005.

E. Pindza, K.C. Patidar, and E. Ngounda. Implicit-explicit predictor-corrector methods combined with improved spectral methods for pricing European style vanilla and exotic options. *Electronic Transactions on Numerical Analalysis*, 40:269–293, 2013.

D. M. Pooley, K. R. Vetzal, and P. A. Forsyth. Convergence remedies for non-smooth payoffs in option pricing. *J. Comp. Fin.*, 6(4):25–40, 2003.

K. Spanderen. Finite Difference Schemes for the Heston-Hull-White Model. https://hpc-quantlib.wordpress.com/2011/09/11/finite-difference-schemes-for-the-heston-hull-white-model/, 2011.

D. Tavella and C. Randall. *Pricing Financial Instruments: The Finite Difference Method.* Wiley, New York, 2000.

T. W. Tee and L. N. Trefethen. A rational spectral collocation method with adaptively transformed Chebyshev grid points. *SIAM J. Scientific Computing*, 28(5):1798–1811, 2006. doi: 10.1137/050641296. URL http://dx.doi.org/10.1137/050641296.

L. N. Trefethen. *Spectral methods in MatLab.* Society for Industrial and Applied Mathematics, Philadelphia, PA, USA, 2000. ISBN 0-89871-465-6.

R. Zvan, P.A. Forsyth, and K. R. Vetzal. Penalty methods for American options with stochastic volatility. *J. Comput. Appl. Math.*, 91(2):199 – 218, 1998. ISSN 0377-0427. doi: http://dx.doi.org/10.1016/S0377-0427(98)00037-5. URL http://www.sciencedirect.com/science/article/pii/S0377042798000375.

Appendix

	method	grid N, Δ_t	error	comp. time [s]
Case 1	Heston FDM	$(1025, 9), 10^{-3}$	2.1320	1.2076
		$(1025, 17), 10^{-3}$	0.2548	2.4379
		$(1025, 33), 10^{-3}$	0.0427	4.7981
		$(1025, 65), 10^{-3}$	0.0093	9.3047
		$(1025, 129), 10^{-3}$	0.0022	19.3582
		$(1025, 257), 10^{-3}$	0.0005	42.6747
	Heston FDM/SP	$(1025, 9), 10^{-3}$	0.2854	2.5891
		$(1025, 17), 10^{-3}$	0.0197	8.2178
		$(1025, 33), 10^{-3}$	0.0007	29.0321
	HHW FDM	$(513, 9), 10^{-3}$	1.3681	8.0264
		$(513, 17), 10^{-3}$	0.2126	29.9697
		$(513, 33), 10^{-3}$	0.0405	120.2508
		$(513, 65), 10^{-3}$	0.0091	516.6477
		$(513, 129), 10^{-3}$	0.0021	2000.1183
	HHW FDM/SP	$(513, 9), 10^{-3}$	0.4541	14.6318 (39.9371)
		$(513, 17), 10^{-3}$	0.0544	88.2399 (147.9660)
		$(513, 33), 10^{-3}$	0.0045	665.2016 (885.5111)
Case 2	Heston FDM	$(1025, 9), 10^{-3}$	3.0133	1.2060
		$(1025, 17), 10^{-3}$	0.2696	2.4897
		$(1025, 33), 10^{-3}$	0.0485	4.7412
		$(1025, 65), 10^{-3}$	0.0105	9.1844
		$(1025, 129), 10^{-3}$	0.0024	20.4079
		$(1025, 257), 10^{-3}$	0.0006	41.9270
	Heston FDM/SP	$(1025, 9), 10^{-3}$	2.6791	2.5921
		$(1025, 17), 10^{-3}$	0.1636	8.2551
		$(1025, 33), 10^{-3}$	0.0015	29.4134
	HHW FDM	$(513, 9), 10^{-3}$	2.2588	8.0193
		$(513, 17), 10^{-3}$	0.2357	29.5823
		$(513, 33), 10^{-3}$	0.0508	120.2891
		$(513, 65), 10^{-3}$	0.0116	510.3783
		$(513, 129), 10^{-3}$	0.0027	2017.8052
	HHW FDM/SP	$(513, 9), 10^{-3}$	3.0757	14.5333 (44.4898)
		$(513, 17), 10^{-3}$	0.2008	88.4106 (157.3312)
		$(513, 33), 10^{-3}$	0.0027	671.1661 (885.4324)
Case 3	Heston FDM	$(1025, 9), 10^{-3}$	2.2587	3.5285
		$(1025, 17), 10^{-3}$	0.2238	7.4648
		$(1025, 33), 10^{-3}$	0.0449	13.9890
		$(1025, 65), 10^{-3}$	0.0107	27.023
		$(1025, 129), 10^{-3}$	0.0026	57.2715
		$(1025, 257), 10^{-3}$	0.0006	124.6463
	Heston FDM/SP	$(1025, 9), 10^{-3}$	0.1675	7.5804
		$(1025, 17), 10^{-3}$	0.0036	24.3784
		$(1025, 21), 10^{-3}$	0.0006	38.3967
	HHW FDM	$(513, 9), 10^{-3}$	6.7405	23.8552
		$(513, 17), 10^{-3}$	0.9890	88.1528
		$(513, 33), 10^{-3}$	0.2274	367.9543
		$(513, 65), 10^{-3}$	0.0557	1493.2121
		$(513, 129), 10^{-3}$	0.0141	5971.3110
	HHW FDM/SP	$(513, 9), 10^{-3}$	0.6566	43.1364 (111.2024)
		$(513, 17), 10^{-3}$	0.0383	259.7538 (475.9415)
		$(513, 33), 10^{-3}$	0.0013	1974.5181 (2612.4923)
Case 4	Heston FDM	$(1025, 9), 10^{-3}$	1.4285	0.6277
		$(1025, 17), 10^{-3}$	0.1632	1.2631
		$(1025, 33), 10^{-3}$	0.0295	2.4344
		$(1025, 65), 10^{-3}$	0.0061	4.6923
		$(1025, 129), 10^{-3}$	0.0014	10.7607
		$(1025, 257), 10^{-3}$	0.0003	21.6599
	Heston FDM/SP	$(1025, 9), 10^{-3}$	0.4379	1.3338
		$(1025, 17), 10^{-3}$	0.0513	4.2569
		$(1025, 33), 10^{-3}$	0.0002	15.0474
	HHW FDM	$(513, 9), 10^{-3}$	1.2024	4.081308
		$(513, 17), 10^{-3}$	0.1541	15.121876
		$(513, 33), 10^{-3}$	0.0339	60.777343
		$(513, 65), 10^{-3}$	0.0081	256.943911
		$(513, 129), 10^{-3}$	0.0027	1022.625657
	HHW FDM/SP	$(513, 9), 10^{-3}$	0.4859	7.431475 (15.9646)
		$(513, 17), 10^{-3}$	0.0400	45.751409 (74.6460)
		$(513, 33), 10^{-3}$	0.0014	339.340268 (418.6251)

Table A1: Convergence results numerical experiments in v,r-direction (Figures 12 - 15). The timings in brackets are the test cases with $\rho_{13}, \rho_{23} \neq 0$.